Published in final edited form as:
Phys Chem Chem Phys. 2009 February 7; 11(5): 748. doi:10.1039/b813817f.

How to turn your pump–probe instrument into a multidimensional spectrometer: 2D IR and Vis spectroscopies *via* pulse shaping

Sang-Hee Shim and **Martin T. Zanni***
Department of Chemistry, University of Wisconsin-Madison, Madison, WI 53706-1396, USA

Abstract

We have recently developed a new and simple way of collecting 2D infrared and visible spectra that utilizes a pulse shaper and a partly collinear beam geometry. 2D IR and Vis spectroscopies are powerful tools for studying molecular structures and their dynamics. They can be used to correlate vibrational or electronic eigenstates, measure energy transfer rates, and quantify the dynamics of lineshapes, for instance, all with femtosecond time-resolution. As a result, they are finding use in systems that exhibit fast dynamics, such as sub-millisecond chemical and biological dynamics, and in hard-to-study environments, such as in membranes. While powerful, these techniques have been difficult to implement because they require a series of femtosecond pulses to be spatially and temporally overlapped with precise time-resolution and interferometric phase stability. However, many of the difficulties associated with implementing 2D spectroscopies are eliminated by using a pulse shaper and a simple beam geometry, which substantially lowers the technical barriers required for researchers to enter this exciting field while simultaneously providing many new capabilities. The aim of this paper is to provide an overview of the methods for collecting 2D spectra so that an outsider considering using 2D spectroscopy in their own research can judge which approach would be most suitable for their research aims. This paper focuses primarily on 2D IR spectroscopy, but also includes our recent work on adapting this technology to collecting 2D Vis spectra. We review work that has already been published as well as cover several topics that we have not reported previously, including phase cycling methods to remove background signals, eliminate unwanted scatter, and shift data collection into the rotating frame.

1. Introduction

Among the spectroscopic tools available for studying molecular structures and kinetics, two-dimensional infrared (2D IR) spectroscopy is unique in its combination of structural and dynamical resolution.[1–3] Its structural sensitivity stems from couplings that link vibrational modes to create molecular vibrations that can extend over many bond lengths. These delocalized modes are often used to globally assess molecular structures such as in peptides and proteins where infrared spectroscopy is commonly used to estimate secondary structures like α-helices and β-sheets.4 Bond specific structural resolution can also be gained by isotope labelling individual or pairs of bonds.[5,6] The structural sensitivity of 2D IR spectroscopy is complemented by an intrinsic dynamical resolution that is on the order of femtoseconds when it is used to study lineshapes and picoseconds when measuring vibrational couplings.[7–9] This time-resolution is sufficient to monitor all but the fastest structural motions. For slower kinetics, 2D IR spectroscopy can be used in a “snapshot” mode to monitor the kinetics of evolving ensembles spanning timescales from picoseconds to seconds or longer.[10] Taken together, it is this unique combination of femtosecond/picosecond time-resolution and global/bond specific

zanni@chem.wisc.edu.

structural resolution that make 2D IR spectroscopy distinct from traditional structural tools such as NMR, X-ray crystallography, electron spin resonance spectroscopy and fluorescence. It is also why 2D IR spectroscopy is now being used in a diverse set of fields such as sub-millisecond protein folding, membrane peptide structure assessment, amyloid fiber formation, chemical exchange, and solvent dynamics, to name a few.[1–3]

While 2D IR spectroscopy has the potential to impact many different fields, it is currently only being used by a relatively select set of dedicated researchers, largely because it has been technically challenging to implement. However, recent advances in mid-IR pulse shaping have significantly reduced the technical hurdles associated with its implementation, making it easier for non-experts to assemble and operate their own spectrometers.[11,12] Moreover, the new shaping approach to collecting 2D IR spectra adds many new capabilities that are not easily implemented with the original methods. Thus, while there will certainly be future advances in the technology and theory of 2D IR spectroscopy, the technique has now progressed to the point where the focus is shifting from technological advances to scientific applications.

This review is aimed at those researchers who are considering whether 2D IR spectroscopy will help their research program, and if so, what experimental approach should be used. Towards this aim, we review the information content of the technique and the technological hurdles associated with its implementation. We then compare and contrast the three ways of collecting 2D IR spectra: hole-burning, heterodyned four-wave mixing, and mid-IR pulse shaping, so that the reader can ascertain which method would best fit their needs. As will become evident, we are strongly biased towards our pulse shaping method for collecting 2D IR spectra. Since inventing this method, we have found few drawbacks and many advantages. In fact, the pulse shaping method can be used to mimic the other two techniques. In sections 5 and 6 of this review, we provide examples of experiments which would be extremely difficult to perform with the other two techniques for collecting 2D IR spectra.

This review is focused on 2D IR spectroscopy, but in collaboration with Niels Damrauer and his group at the University of Colorado-Boulder, we also recently extended our pulse shaping approach to 2D visible (2D Vis) spectroscopies [13] which are being used to explore the electronic couplings and energy transfer processes in photo-biological systems and semiconductors.[14, 15] While 2D IR and 2D Vis spectroscopies probe very different processes, their implementation is virtually identical. The only important difference is that the wavelength is much shorter in the visible, which puts a stringent requirement on the phase stability of 2D Vis spectrometers. However, this tricky problem is automatically overcome with pulse shaping. In this review, we focus on 2D IR spectroscopy, but because the infrared and visible techniques are so similar, our review can also be used to understand pulse shaping methods for collecting 2D Vis spectroscopies as well. To aid in the comparison, we have also included a section on 2D Vis spectroscopy that outlines salient differences.

2. Information content of 2D IR spectra

There are two basic pieces of structural information available from 2D IR spectroscopy: vibrational couplings and line-shapes. Vibrational couplings are measured by the frequency positions of the diagonal and cross peaks in 2D IR spectra, while lineshapes are quantified by the two-dimensional shapes of the peaks. This review is aimed at those researchers who have already decided that the information content of 2D IR or Vis spectroscopies would benefit their research, but do not fully understand the strengths and weaknesses of the various experimental approaches to collecting the data. Thus, we only provide an extremely brief overview of lineshapes and couplings and refer the reader to other review articles for a more comprehensive description on the origin of the diagonal and cross peaks in 2D IR spectra as well as on

additional information that can be extracted such as chemical exchange, energy transfer, and correlations in frequency fluctuations.[1–3]

Couplings between vibrational modes are very good indicators of structure, because they depend sensitively on the relative distances and orientations of bonding groups. Couplings can be measured from linear spectra with a sufficient number of isotopically labelled compounds, but in practice, couplings are more straightforwardly quantified from cross peaks in 2D IR spectra. One way to determine whether two modes are coupled is to pump one mode and probe the response of the other. The magnitude of the response is related to the coupling strength. A 2D spectrum is simply a plot of this response as a function of the pump and probe frequencies. Of course there are much more efficient means of scanning these two frequencies, which is the focus of this article. As an example of a typical 2D IR spectrum, we show in Fig. 1(b) a 2D IR spectrum of a Ni dicarbonyl compound, $Ni_2(PPh_3)_2(CO)_2$ (see Fig. 1a for the structure). This spectrum exhibits 4 pairs of out-of-phase peaks, two along the diagonal and two sets of cross peaks. The negative peaks (blue) fall at the symmetric and asymmetric stretch normal mode frequencies (In wet THF and the presence of air, a ligand exchange reaction takes place resulting in the creation of $Ni(CO)_3PPh_3$, which gives a third peak at $\omega_k = 1999\ cm^{-1}$.16) The positive peaks are shifted away from the negative ones by the curvature of the potential, which is related to the coupling *e.g.* when the coupling is zero, the cross peaks cancel because the positive and negative peaks destructively interfere while the separation between the peaks in the diagonal pairs gives the anharmonic shifts of the individual vibrational modes. Thus, by fitting the 2D IR spectrum, the anharmonicities can be extracted and converted to couplings, which are in turn related to molecular structure.[17,18] Currently there is no convention in the 2D spectroscopy community as to either the labels of the axes or the orientation of the contour plot: some researcher use variables t_n while others using τ and T; sometimes the 2D spectra are rotated or flipped along the diagonal. The focus of our article is on using pulse shaper to collect 2D spectra using a "pump–probe" beam geometry, which is why we have chosen ω_{pump} and ω_{probe} for labels and we plot the spectrum using the same orientation as reported in the first experimental 2D IR research paper.[19]

2D IR lineshapes provide a different means for monitoring structures by helping to reveal the heterogeneity and dynamics of the environment surrounding the oscillators. The frequencies of vibrational modes are influenced by their surroundings, whether it is by hydrogen bonding, electrostatics, or any other force that perturbs the molecular potential energy surface. At any one moment in time, these external perturbations (combined with the couplings) generate a particular vibrational frequency. Each molecule in the ensemble may have a different frequency, in which case the linewidth along the diagonal of the 2D IR spectrum represents the structural distribution of the surrounding environment. The antidiagonal width gives the homogeneous linewidth. If the environment moves then the frequencies shift causing the antidiagonal width to increase. Thus, the structural dynamics of the environment can be measured by comparing lineshapes at various delays between the pump and probe pulses. 2D IR lineshape analysis has been a very successful way of probing the dynamics of liquids[20,21] and is also proving to be an extremely powerful means for probing the structure of membrane peptides9 and amyloid fibrils,10,[22,23] among other applications.

Shown in Fig. 2 is a 2D IR spectrum of human Islet Amyloid Polypeptide (hIAPP), $^{13}C^{18}O$-labeled at Leu27. The peptides aggregate into amyloid fibrils composed of stacks of a pair of hairpins. Shown in Fig. 2(a) is a cross-sectional view of the fibril structure obtained with solid-state NMR[24] that highlights the backbone of Leu27. The lineshape of the label peak at $\omega_{probe} = 1585\ cm^{-1}$ (enclosed with red box in Fig. 2(b)) reflects the environment of the label within the fibril (Fig. 2(a)). For instance, labels in the β-sheets or in the hydrophobic core give round lineshape; labels exposed to the aqueous environment result in diagonally elongated lineshape since surrounding water molecules interact with the label. In principle, one can

determine both the width of the structural distribution and the timescales of motion by lineshape analysis of the linear absorption spectrum, but in practice 2D IR spectroscopy or a related photon echo measurement is necessary.

There are a variety of pulse sequences that can be used to generate 2D IR spectra.[25–27] The spectra shown in Fig. 1 and 2 have the highest frequency resolution possible, because they were generated by collecting both a rephasing and non-rephasing signal, which were then added to produce absorptive line-shapes. When only one set of signals is measured (usually the rephasing), magnitude spectra are usually plotted. Magnitude spectra are less desirable because they have much broader linewidths and the signs of the peaks are not resolved. Real-spectra can be plotted instead, but have lineshapes that are distorted by phase-twist. As a result, absorptive spectra are usually preferable for 2D IR spectroscopy.[28] However, proper addition and phase calibration of the rephasing and non-rephasing signals is not trivial.29 One of the advantages of the pulse shaping method described below, is that properly phased absorptive spectra like those presented above are generated automatically.

3. Methods for collecting 2D IR spectra

In principle, the structural and dynamical information described above is contained in 2D IR spectra no matter how the spectra are generated experimentally, but in practice the method of data collection can influence the ease and accuracy with which the desired information can be extracted.12,[30] There are three main approaches for collecting 2D IR spectra. These are: (1) hole-burning; (2) pulsed four wave mixing; and (3) pulse shaping in conjunction with a partly collinear beam geometry, the last of which is the main focus of this review article. No matter the method, all three are third-order spectroscopies, which mean that there are three interactions between the pulse sequence and the sample. If these interactions occur at the absolute times t_1, t_2 and t_3, then the electric field emitted by the sample, $E^{(3)}(t)$ is thus the 3rd-order system response, $R_n(t_1, t_2, t_3)$, (which contains the desired structural information) convoluted with the electric fields of the pulse train *via*

$$\begin{aligned} E^{(3)}(t) = & \left(\frac{i}{\hbar}\right)^3 \int dt_3 \int dt_2 \int dt_1 \sum_n R_n(t_1, t_2, t_3) E_3(t - t_3) e^{-i\omega(t-t_3)} \\ & \times E_2(t - t_3 - t_2) e^{-i\omega(t-t_3-t_2)} E_1^*(t - t_3 - t_2 - t_1) e^{i\omega(t-t_3-t_2-t_1)} \\ & \times e^{i(+k_3+k_2-k_1)} e^{-i(+\phi_3+\phi_2-\phi_1)} \end{aligned} \quad (1)$$

where E_n are the envelopes, ϕ_n are the phases, and k_n are the wavevectors (directions) of the n-th laser pulse and the summation is over all the possible signals arising from the Feynman pathways, such as the rephasing and nonrephasing signals.[31,32] Note that the complex conjugates on E as well as the signs of ϕ and k in eqn (1) are chosen for the rephasing signal. Other signals, like those that arise from non-rephasing and two-quantum processes (which are discussed below), change the complex conjugates and signs of E_n, ϕ_n and k_n accordingly. Phase sensitive detection is also necessary, which is achieved by heterodyning $E^{(3)}(t)$ with a fourth laser pulse with the same wavevector as the emitted field, which we refer to as the local oscillator, *e.g.*[33]

$$S(\tau, T, t) = \int dt_4 |E^{(3)}(\tau, T, t_4) + E_4(t - t_4)|^2 \quad (2)$$

While absolute times are often used in the derivation of $E^{(3)}(t)$, relative times are more intuitive when discussing pulse sequences, which is why eqn (2) uses the variables $\tau = t_1$, $T = t_1 + t_2$ and $t = t_1 + t_2 + t_3$. Relative times (*e.g.* pulse delays) are defined graphically in Fig. 3 for the various pulse sequences discussed in this article. In 2D spectroscopy, the system response is correlated along two of the dependent variables in the system response. The correlation is most

often between τ and *t* and the results displayed in the frequency domain. The difference in the three experimental approaches for collecting 2D IR spectra lies in how this correlation is performed.

In hole-burning, a pump–probe beam geometry is used where the pump serves as both the E_1 and E_2 pulses and the probe is both the E_3 and E_4 pulses (Fig. 3a) (thus, $\tau = t = 0$).[19] The system response along *t* is measured in the frequency domain using a spectrometer to give the frequency axis ω_{probe}. The response along t is also measured in the frequency domain by scanning the center frequency of the pump beam to give ω_{pump}. To achieve spectral selectivity in the hole burning approach, the bandwidth of the pump beam must be narrowed to less than the homogeneous linewidth of the sample, which is typically accomplished with an etalon, resulting in a picosecond pump beam.[34] The probe beam is a femtosecond pulse so that the bandwidth covers the spectral region of interest. Thus, the hole burning approach to collecting 2D IR spectra operates solely in the frequency domain.

In contrast to hole burning, the pulsed four wave mixing method for collecting 2D IR spectra solely containing femtosecond pulses, operates either wholly or partly in the time domain, and uses a beam geometry where the wavevectors of all four pulses differ (Fig. 3b).[35] The response along ω_{probe} can be measured directly in the frequency domain like the hole burning analog, or in the time domain by scanning *t* and then numerically Fourier transforming the data. The ω_{pump} axis is generated by Fourier transforming the signal as a function of τ. Since the ω_{probe} axis can be collected all at once using a spectrometer and a multichannel detector, data collection is much faster when the Fourier transform is done optically.[36] We refer to this method as four wave mixing to emphasize the non-collinear beam geometry, but of course hole-burning is a four wave mixing technique as well.

The strengths and weakness of the two techniques above have become apparent over the past few years. The hole burning approach is the easiest to experimentally implement since it only requires two laser beams, while the four wave mixing approach requires spatially and temporally overlapping three laser beams in the sample and a fourth on top of the emitted response. The additional pulses in the four wave mixing setup makes it a much more difficult technique to implement, since mid-IR frequencies are invisible to the human eye and can only be measured with bulky detectors. 2D spectra collected using hole burning are also easier to collect and require little post processing of the data, which is a result of the pump–probe beam geometry. Another difference between the hole burning and four wave mixing approaches is that the hole burning technique results in absorptive 2D IR spectra. Absorptive 2D IR spectra are desirable because they have the narrowest linewidths and are not distorted by phase twist. To understand this difference, we must describe the signals that are measured by a 3rd-order response.

The 3rd-order molecular response is the sum of three signals, which we refer to as the rephasing, non-rephasing, and two-quantum signals

$$R_n(t_1,t_2,t_3) = R_n^{\text{rephase}}(t_1,t_2,t_3) + R_n^{\text{nonrephase}}(t_1,t_2,t_3) + R_n^{\text{two-quantum}}(t_1,t_2,t_3) \quad (3)$$

where each term in the summation corresponds to a different Feynman pathway that creates a peak in the 2D IR spectrum. These terms contain processes that are commonly referred to as ground state bleaching, stimulated emission, and excited state absorption. The highest frequency resolution is obtained when both the rephasing and non-rephasing signals are measured and added, as was discussed in section 2 above. This step is necessary because each spectrum contains a twisted phase that broadens the peaks, but cancels when the two spectra

are added to give absorptive spectra.[28] In the four wave mixing geometry, the rephasing and non-rephasing signals are emitted from the sample in different spatial directions due to wave vector matching. For instance, if the pulses arrive at the sample in the order of k_1, k_2 and k_3, then the rephasing signal is emitted in the $-k_1 + k_2 + k_3$ direction while the non-rephasing signal appears in the $+k_1 - k_2 + k_3$ direction. Since measuring both directions simultaneously would require an additional local oscillator pulse, the two signals are usually measured in the same phase matching direction, by reversing the ordering of the k_1 and k_2 pulses and thereby swapping the roles of the E_1 and E_2 pulses in eqn (1); *e.g.* the rephasing signal is measured first by scanning the delay when k_1 impinges on the sample before k_2, and then measuring the non-rephasing signal by again scanning the time delay when k_2 reaches the sample first. Once the spectra have been collected, they must be phased and added.[29] Phasing is necessary because it is exceedingly difficult to experimentally set the time zeros of the laser pulses (an offset in the time domain is equivalent to a phase shift in the frequency domain), so the spectra are compared to a transient pump–probe spectrum for which the t_1 and t_3 are precisely zero because both E_1 and E_2 come from the pump and E_3 and E_4 come from the probe.[29] (The reader can summarize the difficulty of these tasks simply by the amount of text taken to qualitatively describe the process!) This elaborate process is in contrast to 2D IR spectroscopy *via* hole burning. Since the hole burning approach has a pump–probe phase matching geometry, the rephasing and the non-rephasing are emitted collinearly and are automatically phased because the time-zeros are precisely zero, resulting in the desired absorptive spectrum. No post data processing is necessary for the hole burning approach and only half the number of 2D IR scans need be collected as compared to the four wave mixing geometry since both the rephasing and non-rephasing spectra are collected simultaneously.

An additional advantage of the hole burning approach is that a portion of the 2D IR spectrum can be monitored without having to collect an entire 2D IR spectrum. For instance, an individual cross peak can be measured by tuning to the appropriate pump frequency, whereas in the four wave mixing approach, the cross peaks are not resolved until after the data is collected and Fourier transformed. This ability is sometimes advantages when monitoring kinetics such as during protein folding. There are also no problems with phase-drift when using hole-burning. In the four-wave mixing approach, beam pointing and pathlength variations cause a drift in phase which either needs to be actively stabilized,[37] measured and corrected,[38] or through passive stabilization. [39,40] Phase drift is especially problematic in the visible because of the short wavelength. An advantage of 2D IR *via* four wave mixing is that the signal is background free and thus has higher sensitivity. It also has better frequency and time-resolution, because only femtosecond pulses are used where as hole burning requires a picosecond pulse. Moreover, this method provides superior selectivity of choosing a specific signal by spreading combinations of excitations in space according to their phase matching conditions and by controlling polarizations of all four pulses to selectively allow a combination of transitions at a specific order of angles. We come back to this point shortly.

4. Overview of 2D IR spectroscopy *via* pulse shaping

We now turn to the focus of this review article, which is the third method for collecting 2D IR spectra (Fig. 3c).[12] It is in many ways a combination of the above two methods. It uses a pump–probe beam geometry like the hole burning approach, but uses two femtosecond pulses for the pump beam like the four wave mixing approach. Using the pulse shaper, the τ delay is scanned like the four wave approach and the signal Fourier transformed so that the optimal time and frequency resolution is obtained. Furthermore, the spectra are automatically phased because the shaper can perfectly set the τ time delay and the t time delay is zero by default. Thus, the best possible 2D IR spectrum is collected automatically without complicated and potentially erroneous post data processing, as we describe in more detail below.

This third method for collecting 2D IR spectra is made possible by a pulse shaper that we recently developed that operates in the mid-IR.[11,41] Shown in Fig. 4 is a schematic of our pulse shaper as well as the spectrometer. A small fraction of the input IR beam is served as a probe, and the remainder is sent to the shaper and serves as a pump. The pulse shaper (gray area enclosed with a dashed line) consists of two gratings and two cylindrical mirrors in a 4-*f* geometry, typically used in visible pulse shapers, and an acousto-optic modulator made of germanium. The first grating and cylindrical mirror serve to disperse and collimate the frequency components of the incident mid-IR pulses along the length of the germanium crystal. The pulse is shaped by an acoustic wave that propagates along the length of the crystal, whose time-dependent amplitude and phase can be set with an arbitrary waveform generator in an attached computer. Since the acoustic wave propagates slowly through the crystal as compared to the femtosecond mid-IR pulse, the wave acts as a programmable grating, deflecting the desired mid-IR frequencies with specified intensity and phase.[42] The second grating and cylindrical mirror serve to transform the deflected frequencies back into the time domain. Thus, to create a desired optical pulse in time domain, one just needs to calculate its Fourier transform and feed it to the acousto-optic modulator as an acoustic wave (several calibration steps are also necessary). Mathematically, the electric field of the shaped pulse in frequency is the product of the incident electric field and a mask function of the acousto-optic modulator:[43]

$$E_{\text{out}}(\omega) = E_{\text{in}}(\omega)\, M(\omega) \tag{4}$$

where the electric fields and the mask are complex functions in frequency. In this manner, all that is needed is some simple programming to delay an input pulse in time, to create two pulses or an entire pulse train from a single input pulse, to mimic an optical component such as an etalon, or to create any frequency/time domain pulse within the limits of the shaper resolution.

To demonstrate the utility of collecting 2D IR spectra with our shaper, in what follows we show a series of 2D IR spectra that have been collected with differently shaped pulse sequences. We start by mimicking the hole burning approach and then sequentially optimize the spectra with improved pulse sequences. Shown in Fig. 5 are four series of 2D IR spectra collected for $W(CO)_6$ solvated in n-hexane, which is a model compound that has a single IR active antisymmetric stretch near 5 microns. Each series is generated using a different pump shape.

The first series of 2D IR experiments mimic the spectra that would be generated had an etalon been used to narrow the pump spectrum, like in the hole-burning method described above. An etalon consists of two partial reflectors aligned parallel so that a pulse entering on one end bounces back and forth between the two mirrors, leaking a portion of the pulse with each bounce. The leaked portions interfere with one another, creating a narrow-band whose center frequency is determined by the distance between the two mirrors, *d*, according to

$$M(\omega) = \frac{1 - R}{1 - R \cdot \exp[+i(2d\cos\theta/c)\omega]} \tag{5}$$

where *R* is the reflection coefficient, θ is the angle the light travels through the etalon and *c* is the speed of light.[44] To generate the 2D IR spectra in the first row of Fig. 5, we set the bandwidth to 4.6 cm^{-1} (which is slightly larger than the homogeneous linewidth of 4.4 cm^{-1}), scanned *d*, and plotted the change in absorption of the probe with and without the pump. 2D IR spectra were collected at two different pump–probe delay times, $T = 2000$ and 200 fs. At $T = 2000$ fs, a negative and a positive peak pair is observed (blue and red in Fig. 5, respectively), which is exactly as expected according to standard hole burning approaches on metal carbonyl systems. The negative peak appears along the diagonal with $\omega_{\text{pump}} = \omega_{\text{probe}} = 1983$ cm^{-1}, which is the

fundamental frequency of $W(CO)_6$. The positive peak is shifted by $\Delta\omega_{probe} = 13.3\ cm^{-1}$, which is the anharmonicity of the $W(CO)_6$ antisymmetric stretch.[45] The spectra contain all of the desirable characteristics about hole-burning that we discussed above: it is properly phased without any post-data corrections and the peaks have absorptive lineshapes. Thus, pulse shaping can reproduce the data collected using an etalon. But, what the spectra themselves do not reveal, is that in practice, it is easier and faster to collect the 2D data set using pulse shaping rather than an etalon. An etalon consists of two high reflective mirrors whose relative distance sets the center frequency of the narrow pulse. Because displacements of ~10 nm are needed to scan the center frequency by 1 cm^{-1}, piezo crystal actuators are typically used.[30] Piezo crystal actuators are slow and not reproducible. Thus, at each point during scanning, the pump pulse frequency is set using feedback from a spectrometer, which is time consuming. In contrast, once the pulse shaper is calibrated, the center frequency and shape can be set with simple programming and does not need to be checked since a frequency band of 1 cm^{-1} corresponds to a window of ~100 μm on the crystal aperture, which is straightforward to locate precisely. Furthermore, the pulse shape can be changed with every laser shot, so there is no dead time associated with changing frequencies. As a result, data collection is much faster and easier.

A significant drawback of the hole burning approach is that the picosecond pump pulse can distort the signal. This distortion becomes larger the smaller the time delay between the pump and probe pulses, which become especially grievous in Fig. 5c at $T = 200$ fs. An etalon narrows the pump pulse bandwidth, but in doing so causes the pulse to have an exponential-like decay in the time-domain (Fig. 5a). Distortions occur when the tail overlaps with the probe, which is why large T delays are required when hole burning is used. Furthermore, the signal strength decreases exponentially with T because of population relaxation. Thus, many applications are best done with T delays as short as possible. Of course, the tail can be minimized by using a shorter duration for the pump pulse, but this leads to a larger bandwidth and poorer frequency resolution in the 2D IR spectra.

Pulse shaping provides alternative approaches for data collection using hole burning. With pulse shaping, the time and frequency profiles of the pump pulse are not limited to just what can be created by an etalon, but can be programmed to optimize the spectral features. For instance, we have collected a series of spectra using a “time-reversed” etalon shown in the second row of Fig. 5, which has a frequency distribution that is identical to an actual etalon, but instead has an exponential tail in the time-domain that decays away from the probe pulse. This shape is simply generated by changing the sign of the phase in the exponential in eqn (5) (*i.e.* $\exp[-i(2d\cos\theta/c)\omega]$). Thus, the pump and probe pulses do not overlap until much shorter T, resulting in smaller peak distortions. Furthermore, the signal strength is also stronger for a time-reversed etalon pulse shape, since the population has had less time to relax with shorter T.

The exponential shape of an etalon has a second disadvantage, which is that it creates Lorentzian lineshape in the frequency domain along the pump axis. This Lorentzian lineshape is a consequence of the spectrum being a convolution of the pump spectrum with the natural linewidth of the molecular vibration. Lorentzian lineshapes have a very broad baseline, and as a result, the 2D peaks have broad tails, which degrades the frequency resolution. An improvement would be to use a pump shape that reaches baseline more quickly. Shown in the third row of Fig. 5 is a series of 2D IR spectra collected with a Gaussian pump pulse. Note that the tails along the pump axis are now much shorter, which is because the Gaussians decay much more rapidly than Lorentzians and thus have improved resolution even for pump pulses with the same full-width-at-half-maximum. Although we have explored Lorentzians and Gaussians here, any number of other frequency-domain shapes could be used.

The fourth method that we report here more closely resembles the pulsed four wave mixing method except that the experiment is performed in a pump–probe beam geometry. In this method, the pulse shaper is used to create two transform limited pulses. Rather than scan the frequencies like was done above, the 2D IR spectrum is instead generated by collecting the signal as a function of the time delay between the two pump pulses, τ, and Fourier transforming it to give the ω_{pump} axis. Any function gets shifted in time by τ when its counterpart in frequency is multiplied with $\exp(i\omega\tau)$, then inversely Fourier-transformed. Thus, a mask function for a pulse pair with one pulse at $t = 0$ and another pulse at $t = \tau$ can be written as

$$M(\omega)=\frac{1}{2}(e^{i\omega\tau}+1) \tag{6}$$

where the latter term generates the pulse at $t = 0$ and the former term generates the pulse at $t = \tau$. Eqn (6) can be rearranged as

$$M(\omega)=\cos(\omega\tau/2)e^{i\omega\tau/2} \tag{7}$$

Thus, combining an amplitude mask of $\cos(\omega\tau/2)$ and a phase mask of $\omega\tau/2$ generates a pulse pair composed of one pulse fixed in time and a second pulse that arrives τ earlier. In this manner, the τ delay is scanned without altering T. The mask in eqn (7) sets the phases of the two pump pulses inside their respective envelopes zero ($\phi_1 = \phi_2 = 0$), mimicking the way that pulse delays are typically generated using translational stages. The resulting spectra are shown in the fourth row of Fig. 5 for $\tau = 0$ to 10 000 fs in 14 fs steps. Like the first three methods, the spectra are automatically phased and have absorptive lineshapes, but now the narrowest $W(CO)_6$ pump linewidth is measured and there is no discernable distortion in the peaks down to $T = 50$ fs (the fwhm of the pulses). Thus, we are able to generate the ideal 2D IR spectrum in a straightforward manner. As was explained in section 2, this fourth method retains the phasing and absorptive features of the pump–probe spectra because both rephasing and non-rephasing signal are collected simultaneously and the time-zeros of the pulse delays are perfectly set, resulting in a properly phased spectrum. Moreover, femtosecond pump pulses allow linewidths closest to the intrinsic resolution to be measured. We also point out that the peak shapes are symmetrical about ω_{pump} and that there are no spurious ghost images, indicating that the shaper time-resolution is sufficiently accurate to collect high-resolution spectra. Asymmetric shapes and ghost images are common problems that occur when 2D IR spectra are collected using translational stages to increment time delays.[37,38]

Our mid-IR pulse shaper is well-suited to generate pulse sequences for 2D IR experiments.[11,41] The actual resolution is 190 equivalent pixels, which enables us to generate a pulse pair with a time delay as large as 13 ps. The Ge AOM itself is designed for a resolution of 500 pixels, which can be achieved by focusing the frequencies into the crystal more tightly, in which case we can generate delays as large as 35 ps. The shaper was also demonstrated to generate pulse pairs with relative phases within an accuracy of 0.008π rad[11] that is perfectly stable for hours. High phase stability between the pulses occurs because the two pump pulses pass through the exact same optical setup. Moreover, their absolute phases are stable within $\lambda/27$ relative to an unshaped pulse over 100 s.[41] This level of absolute phase stability means that the shaper is not limited in pulse sequences and phase matching geometries where phase differences matter, but could be used to shape only a single pulse in a pulse train (in a box car geometry, for instance) or that two shapers could be used in conjunction. Thus, there are many possible variations that could be straightforwardly implemented in the future. Of the four pulse sequences we have explored to date using our shaper, the pulsed method has the best time and frequency resolution, and so we focus on this method for the rest of this article.

5. Phase control in pulse shaping 2D IR spectroscopy

Besides setting the time-dependent amplitudes of the pulses, the shaper also allows arbitrary control over the phase. The pulse shaping mask in eqn (6) for a pulse pair can be extended with additional phase terms;

$$M(\omega)=\frac{1}{2}[\exp(i\omega\tau)\exp(i\phi_1)+\exp(i\phi_2)] \quad (8)$$

where ϕ_1 and ϕ_2 are the phases of the pulse at $t = \tau$ and 0, respectively. Any functional form in frequency can be given for ϕ_1 and ϕ_2. The phase of the pump pulses also affects the phase of the emitted response (*e.g.* measured 2D IR signal). In a pump–probe geometry, two phase matching directions of $-k_1 + k_2 + k_3$ and $+k_1 - k_2 + k_3$ are detected, so the phase of the signal, ϕ_{sig}, can be written as

$$\phi_{sig}=\pm(\phi_1-\phi_2)+\phi_{probe}-\phi_{probe}=\pm(\phi_1-\phi_2) \quad (9)$$

Thus, the 2D IR signal depends on the relative phase between the pulses in a pulse pair, $\Delta\phi_{12}$, according to eqn (1). For example, if the phase of the first pulse in the pulse pair is rotated by π, so will the signal. Using this fact, we routinely implement phase incrementing or phase cycling to shift the signal to a lower frequency, remove the unwanted transient absorption background, and subtract scatter from the signal. In this section, we outline each of these capabilities and describe the pulse sequence most often used in our group.

5.1. The rotating frame

As described by eqn (1) and (9), the phase of the emitted signal depends on both τ and $\Delta\phi_{12}$. If these two equations are combined, then the emitted field $E_n(t)$ depends on τ and $\Delta\phi_{12}$ according to $E_n(t;\tau)\propto \exp(-i\tau\omega_0 + i\Delta\phi_{12})$. Thus, when τ is incremented by half the period of the fundamental frequency, the phase of the emitted signal flips. However, $\Delta\phi_{12}$ can be used to partially or wholly counteract the phase flip, which results in a shift of the observed frequencies. Since the fundamental frequencies are already known from the linear spectrum, it is not important to measure their absolute values with 2D IR spectroscopy, but only their difference. As a result, data collection is faster because fewer data points are necessary to characterize the signal (the Nyquist frequency is extended). In the extreme limit, the measured signals are aliased all the way to zero frequency. This process of shifting the observed frequency is equivalent to making the measurements in a rotating frame.[46,47]

Fig. 6 demonstrates the rotating frame with time scans along τ measured for *N*-methylacetamide (NMA), which is commonly used as a model for peptide linkages, in D_2O. When no rotating frame is used, $\Delta\phi_{12} = 0$, and the 2D IR signal oscillates at ω_0 alongτ, which is illustrated in the top panel of Fig. 6a (NMA in D_2O has a period of 21 fs corresponding to $\omega_0 = 1625$ cm^{-1}). To rotate the frame, the observed signal frequency is shifted by incrementing $\Delta\phi_{12}$ with the time delay, *i.e.* $\Delta\phi_{12} = -\omega_i\tau$ where ω_i is a constant parameter. Then, the phase increment has the effect of shifting the frequency of the emitted signal to $\omega_0 - \omega_i$. When $0 < \omega_i < \omega_0$, the signal frequency has a period larger than 21 fs (Fig. 6a, middle for $\omega_i = 1200$ cm^{-1}, corresponding to a period of 78 fs) and in the extreme case when $\omega_i = \omega_0$, the observed signal no longer oscillates with τ (Fig. 6a, bottom). To test the accuracy of this procedure we performed a series of measurements to correlate ω_I with the frequency shift (Fig. 6b). The correlation is linear with a slope of −0.99 and an rms of 2.0 cm^{-1}, indicating that our shaper quite accurately increments the phase.

The time scans reported in Fig. 6 were measured using several hundred points to clearly illustrate the frequency shift, but in practice only two points are needed per period according to the Nyquist frequency (actually, a little more than 2 points per period are needed to account for the pulse bandwidth), [48] and so data collection is more rapid. For instance, in the amyloid work described below in section 6, we used a sampling scheme of $\omega_i = 1225\ \mathrm{cm}^{-1}$ and a time step of 22 fs. This choice was made by considering how far from zero-frequency we wanted to measure the signal (since the noise is progressively higher at lower frequencies), the amount of time we want to scan (primarily set by the vibrational dephasing rate) and how many data points we want to collect (which is based on the memory size of the arbitrary waveform generator and the number of phase cycles being used). Undersampling can also be used to make similar choices. Phase cycling wholly or partially into the rotating frame is extremely convenient and is especially powerful when combined with schemes to reduce background noise, which is explained below.

5.2. Removing transient absorption background

According to eqn (1), the 3rd-order signal is generated by two interactions with the pump pulse (E_1 and E_2) and one interaction with the probe (E_3). However, a 3rd-order signal is also generated when E_1 or E_2 interacts twice with the sample (like in a typical pump–probe experiment), which gives rise to two transient absorption spectra, *e.g.*,

$$S_B(\tau, T, \omega_{\mathrm{probe}}) = \left| \int \mathrm{d}t \sum_n (R_n(\tau, T, t) \otimes E_i^* \otimes E_i \otimes E_{\mathrm{probe}} + E_{\mathrm{probe}}) e^{-i\omega_{\mathrm{probe}} t} \right|^2$$

where $i = 1$ or 2 and $\otimes$s represent convolutions of the electric fields with the response function as in eqn (1). These background signals offset the desired signal, and unless they are removed, cause ringing in the Fourier transformed spectra. When working in the rotating frame they become especially problematic because they cause large intensities near zero-frequency. They can be subtracted during data collection using a chopper, as is standard in pump–probe spectroscopies, or the shaper itself can be programmed to act like a chopper. However, chopping the beam also effectively reduces the repetition rate of the laser, which leads to poorer signal-to-noise. Instead, we use phase cycling to eliminate the background without reducing the repetition rate. We also present in section 7 an alternative method that utilizes the polarization sensitivity of the signals to remove the transient absorption background.

Our scheme is as follows. The phase of desired signal depends on $\Delta\phi_{12}$ whereas the background transient absorption is insensitive to this phase difference. Thus, for each time delay, we collect signal with $\Delta\phi_{12} = 0$ and $\Delta\phi_{12} = \pi$, which we subtract, *e.g.* $S(\Delta\phi_{12} = 0) - S(\Delta\phi_{12} = \pi)$. Thus, signal is collected for every laser shot so that there is no loss of repetition rate. The subtraction procedure is demonstrated in Fig. 7 for NMA in D_2O, where we show the data for each of the signals separately. Fig. 7a displays two time scans of NMA in D_2O at $\omega_{\mathrm{probe}} = 1625\ \mathrm{cm}^{-1}$ when $\Delta\phi_{12} = 0$ (red) and $\Delta\phi_{12} = \pi$ (blue). The oscillation when $\Delta\phi_{12} = \pi$ appeared out of phase to the oscillation when $\Delta\phi_{12} = 0$, while the backgrounds remained the same. Therefore, when the two scans with $\Delta\phi_{12} = 0$ and π are subtracted, the backgrounds are removed, leaving only the desired oscillatory part with double the intensity (green). Fig. 7b displays the resultant spectra after Fourier-transformation giving a peak with the opposite sign for $\Delta\phi_{12} = 0$ (red) and π (blue). Oscillations are apparent in both signals due to the offsets. In contrast, the subtracted signal is double in intensity and free from the oscillatory noise (green). The backgrounds can be numerically subtracted during signal collection, but subtracting the two out-of-phase signals during data collection is preferable, because subtraction can be done every other laser shot, resulting in better cancellation.

5.3. Removing scatter

The transient background absorption signals discussed above are inherent to the partly collinear phase matching geometry being used (except for alternative polarization methods described below). But laser light from the pulses can be scattered off spatially inhomogeneous samples such as crystals, aggregates or any sample with length scales comparable to the wavelength of light. This is an especially grievous problem with membranes and amyloid peptides, which we study in our laboratory, because the vesicles and fibrils span length scales of 30 nm to several microns. Fortunately, much of this scatter can be removed by phase incrementing or cycling. The desired 3rd-order signal arises from each pulse interacting with the sample once, while the scatter occurs from each laser pulse, for $i = 1$ or 2, separately, *e.g.*

$$S_c(\tau, T, \omega_{\text{probe}}) = \left| \int dt (E_i \otimes E_{\text{probe}} + E_{\text{probe}}) e^{-i\omega_{\text{probe}} t} \right|^2 \quad (11)$$

Thus, the phase of the desired signal depends on $\Delta\phi_{12}$, the phase of a background from the scattered pump depends on ϕ_1 or ϕ_2. Thus, by rotating $\phi_1 = \phi_2 = \omega_i\tau$, the signal remains at the same frequency ($\Delta\phi_{12} = 0$) while the scatter frequency is shifted to $\omega_0 - \omega_i$, where ω_0 is the center frequency of the incident mid-IR.

Fig. 8 illustrates this capability on a sample of fibrils from human Islet amyloid polypeptide (hIAPP) in D_2O. hIAPP forms fibrils ~100 nm in diameter and up to several microns in length.[49] As a result, the sample scatters the mid-IR pump, which interferes with the desired spectrum. Scatter from the stationary pulse in the pulse-pair pump can be subtracted or filtered because it appears at the $\omega_{\text{pump}} = 0$. However, postprocessing is not as effective for removing scatter from the moving pulse because this scatter appears along the diagonal axis and overlaps with the desired spectrum (Fig. 8a). Rather than post-correcting our data, we shift the scatter frequency to separate the scatter from the desired spectrum during the experiment. When $\omega_i = 1800\ \text{cm}^{-1}$ is used to increment both ϕ_1 and ϕ_2, the scatter from the stationary pulse moves up to $\omega_{\text{pump}} = 1800\ \text{cm}^{-1}$, while the scatter from the moving pulse shifts to $\omega_{\text{pump}} = -220\ \text{cm}^{-1}$. As a result, the desired 2D spectrum from $\omega_{\text{pump}} = 1580$–$1700\ \text{cm}^{-1}$ is scatter free (Fig. 8b).

The pulse sequence most often used in our lab subtracts off both the transient absorption and background scatter, while shifting the signal into the rotating frame, if desired. We accomplish this by collecting four signals: $S(\phi_1 = 0, \phi_2 = 0)$, $S(\phi_1 = 0, \phi_2 = \pi)$, $S(\phi_1 = \pi, \phi_2 = \pi)$, and $S(\phi_1 = \pi, \phi_2 = 0)$. We then add them in the following order: $[S(\phi_1 = 0, \phi_2 = 0) - S(\phi_1 = 0, \phi_2 = \pi)] + [S(\phi_1 = \pi, \phi_2 = \pi) - S(\phi_1 = \pi, \phi_2 = 0)]$. The result is that the unwanted background scatter and transient absorption signals are subtracted while the signal is additive for all 4 pulse signals. The rotating frame is added by $\phi_1 = \omega_i\tau$, and $\phi_2 = 0$, or any other way that satisfies $\Delta\phi_{12} = \omega_i\tau$. Since each pulse sequence in the series is collected from one laser shot to another, it only takes 4 ms at 1 kHz repetition rate to measure all four signals. On this timescale, the scatter is essentially constant, so that excellent background subtraction is achieved even for aggregating amyloids that create time-dependent scatter intensities.[22]

5.4. Phase cycling to extract the rephasing and non-rephasing spectra

As stated above, a pump–probe beam geometry naturally gives rise to absorptive lineshapes because both the rephasing and non-rephasing spectra are generated collinearly. Absorptive spectra are frequently used in multidimensional experiments because they have the highest frequency resolution and lack phase twist which can distort spectra. But sometimes it is preferable to analyze the rephasing and non-rephasing spectra separately, such as when analyzing the joint frequency fluctuations between coupled chromophores[50] or the dephasing time of coupled systems.[51] A decade ago, Douwe Wiersma and coworkers showed that the rephasing and non-rephasing spectra could be extracted from a collinear geometry by rotating

both the relative phase $\Delta\phi_{12}$ as well as the phase of the probe beam and the local oscillator (*e.g.* $\Delta\phi_{34}$), and adding the spectra together.[52] However, the pulse shaping method described here does not manipulate the probe beam and so the Weirsma method cannot be used. However, Ogilvie and coworkers recently showed that rephasing and non-rephasing spectra can be isolated from spectra collected using a pulse shaper and a partly collinear geometry similar to what is described in this article.[53] Rather than rotate the probe phase, they instead inverse Fourier transform the spectrum measured in the spectrometer, enforce causality, and then combine the necessary real and imaginary components for spectra collected with $\Delta\phi_{12} = 0$ and 90°. Using this trick, rephasing and non-rephasing spectra can now be generated even for pump–probe beam geometries. We applied their approach in the mid-IR using the amide I mode of NMA to generate rephrasing, non-rephasing and magnitude 2D IR spectra, shown in Fig. 9. The method worked very well in the mid-IR. Thus, their procedure eliminates one of the few drawbacks for collecting 2D spectra with pulse shaping and a collinear geometry.

6. Rapid data collection afforded by pulse shaping 2D IR spectroscopy

One of the most important advantages of using pulse shaping and a pump–probe beam geometry is that data collection is extremely rapid. In a traditional 2D IR laser setup, the delay times are adjusted by either changing the pathlengths that the pulses traverse to the sample using a retroreflector on a translational stage or by changing the amount of material the pulses pass through by translating a wedged optic. Translations of this magnitude take roughly 50–100 ms to complete, during which data is not normally collected.[54] Data collection is much more efficient using a pulse shaper to create the pulse sequences because there are no moving parts and the pulse sequences can be changed on a shot-to-shot basis. For our germanium acousto-optic modulator, it takes 10 microseconds for the sound wave to travel the length of the modulator.[11] Thus, a new waveform can be loaded every 10 microseconds, corresponding to a repetition rate of 100 kHz. Thus, at 1 kHz, the time delay is easily incremented at every laser shot, making data collection much faster with a pulse shaper. The improvement in performance will be especially noticeable in the future with higher repetition rate lasers because the data collection rate will increase linearly with repetition rate, unlike systems using translational stages in which the deadtime cannot be redued. Higher repetition rates should also lead to reduced noise reduction by moving the measurement frequency away from the noise frequencies inherent to femtosecond laser systems.

We typically utilize 400 waveforms for a 2D IR data set. These waveforms are uploaded into the memory of the arbitrary waveform generator prior to the experiment (it takes ~40 s to upload the waveforms). We then trigger the experiment, at which point the waveform generator cycles through the loaded waveforms, one at a time, synchronized to the laser repetition rate. Thus, at 1 kHz, an entire 2D IR data set is collected in only 0.4 s. This process is continuously repeated until the necessary signal to noise is achieved. Averaging 100 shots (like in a traditional set), thus takes 40 s.

The fast data collection made possible by pulse shaping allows for an inherently new method for studying kinetics because 2D IR spectra can now by collected on-the-fly. To demonstrate this approach, we show in Fig. 10 the kinetics of amyloid fiber formation followed by continuously scanning 2D IR spectra over several hours.[10] hIAPP aggregates from a random coil form into amyloid fibrils composed of stacked β-sheets (Fig. 10a).[24,55,56] To follow this process, we dissolved denatured hIAPP into buffer and then immediately began collecting 2D IR spectra. We used the 2-phase pulse sequence from section 5.2, so that an entire 2D IR data set was collected every 0.4 s to generate thousands of spectra over the course of three hours. Each individual data set has inadequate signal-to-noise (since it is composed of only 400 laser shots), so we perform a running average to achieve the necessary signal-to-noise. The time-window used in the running average typically spans 1 to 10 min, depending on the signal

intensity of the amyloid. We use shorter time-windows on systems with stronger signals, less scatter and/or larger transition dipoles. Shown in Fig. 10b are three representative 2D IR spectra after a running average of 5 min was used. At t = 1 min, the 2D IR spectrum is of a random coil whose signature is the out-of-phase doublet centered at $\omega_{pump} = \omega_{probe} = 1644$ cm^{-1} and elongated along the diagonal. As the amyloid fibers form, a pair of round peaks shows up at 1618 cm^{-1}, which is the signature of the β-sheets in the amyloid fiber. Thus, the kinetics of random coil and β-sheet can be monitored with these features. From thousands of 2D IR spectra collected during the aggregation, kinetics curves of random coil and β-sheet were constructed in Fig. 10c by simply monitoring the slices along the ω_{pump} = 1644 and 1618 cm^{-1} shown as dotted lines in Fig. 10b from the 2D IR spectra averaged over a 1 min window. The 2D IR spectra can also be fit to extract peak frequencies and shapes, for example (see Fig. 10d). We emphasize that this rapid-scan approach is inherently different means for data collection, since spectral acquisition is limited only by the repetition rate of the laser and a running average can be used after data collection to obtain the optimum signal-to-noise and time-resolution.

7. Polarization and signal strength

Our experience over the past year with collecting 2D IR spectra using pulse shaping *versus* traditional heterodyne methods has led us to conclude that there are very few drawbacks to the technique and many advantages. Nonetheless, there are two places for improvement. The phase cycling scheme in section 5.2 removes the transient absorption background every two laser shots, but because the background is still physically present, it contributes to the noise. Another place for improvement is in the intensity of the probe beam. The pump–probe geometry limits the intensity of the probe beam since the probe needs to be weak enough that it does not saturate the detector, but since it also serves as the third excitation pulse, the signal is not as intense as in a four wave mixing geometry which has a separate local oscillator pulse. Therefore, it would be ideal to truly eliminate the transient absorption background and have a means to independently control the pump and local oscillator intensities. Polarization can improve both these scenarios.

When each polarization of the four pulses are separately controlled, a specific 2D IR signal can be separated from the rest by selectively allowing a certain dipolar combination.[57] So far in the examples of this review, all the three excitation pulses have been polarized parallel to each other, *XXX*, so that the 2D IR signal is generated at the same polarization, *X* .We refer to this polarization scheme as *XXXX*. Since the third excitation beam and the signal have the same polarization, their intensities are linked and limited by the dynamic range of the detector. However, the experiment can be designed so that the emitted field is polarized perpendicular to the third excitation beam (*e.g.* along *Y*). For instance, if the two pump excitation are polarized at 45° (*e.g. X* + *Y*) and the probe along *Y*, then the emitted polarization is along *Y* because (*X* + *Y*) (*X* + *Y*)*XY* = *XYXY* + *YXXY*. Another possibility is to set the three excitation polarizations explicitly to *XYX* in which case only the orientational response *XYXY* is measured. With either of these polarization schemes the signal can be amplified by placing a polarizer before the detector set at *Y* to emit the signal but block the probe (k_3) beam. The amplification occurs because there is now no limit to the probe (k_3) intensity that can be used, since the probe no longer impinges on the detector (In practice, the polarizer much be tilted slightly to let through a little of the probe light for heterodyning purposes).[58] Of these two polarizations, the *XYXY* polarization scheme has the additional benefit that the signal is measured background-free because the background signals are not dipole allowed (*e.g. XXXY* and *YYXY* are both forbidden).

To demonstrate such a scheme, pulse pairs were generated from a Michelson interferometer, of which each arm is equipped with a separate waveplate/polarizer pair. On the probe beam, another waveplate/polarizer pair was placed before the sample and a polarizer after the sample.

In Fig. 11, the 2D IR spectra of acetic acid in chloroform were collected with *XYXY* along with *XXYY*, whose 2D IR intensities are theoretically the same when using the same excitation intensities.[58] When the polarization scheme of *XXYY* used, backgrounds were observed in the time domain data (Fig. 11a) at ω_{probe} = 1703 (blue) and 1716 cm^{-1} (red). The background shown as a solid white line through the center of the oscillation is transient absorption created by each of the individual pump pulses. The signal-to-noise can be seen in Fig. 11b, which shows the Fourier transform of the time-domain data at ω_{probe} = 1703 (blue) and 1716 cm^{-1} (red), which are equivalent to two slices through the 2D IR spectrum. The signal-to-noise is 20 at ω_{probe} = 1716 cm^{-1} and the noise near zero-frequency was large enough to tail throughout ω_{pump}. On the contrary, the time-domain data from *XYXY* (Fig. 11c) were free from the background in *XXXX* and *YYXX*, which was eliminated by the polarizer after the sample set at 85°. (In practice, the emitted field must still be heterodyned, so we tilt the polarizer 5° from *Y* to create the local oscillator). Moreover, the signal was ~5 times more intense (Fig. 11d) because the probe beam could be much more intense without causing saturation of the detector. The noise was also suppressed to give the signal-to-noise of 200 (10× improvement). Also note that the background-free signal minimized the zero-frequency noise component so that the rotating frame can be better utilized. We have also measured spectra using the (45°)(45°)*XY* polarization (unpublished), which is also more intense, but the zero-frequency noise component is not reduced because the transient absorption is still present.

Based on these results, it is clear that a pulse shaper capable of modulating the amplitude, phase and polarization would be ideal for collecting multidimensional infrared and visible spectra. Such a shaper does not yet exist in the mid-IR, but polarization pulse shaping in the visible and near-IR wavelength ranges is now routine.[59,60] Other useful technologies might be incorporated such as upconversion of the mid-IR signal into the visible.[54,61]

8. 2D visible spectroscopy

Our method of collecting 2D spectra is not limited to the infrared. The combination of pulse shaping and a partly collinear beam geometry is also applicable for generating 2D visible (2D Vis) spectra. Pulse shaping has been used previously to collect 2D Vis spectra by generating fully collinear pulse sequences[62] and by both spatially and temporally shaping for added control over wavevector matching.63 However, 2D Vis spectroscopy can be straightforwardly implemented using the protocols described here with a standard visible modulator and a transient absorption optical layout.13 Regardless of which method is used, one of the biggest advantages of using pulse shaping to collect 2D Vis spectra is that it overcomes one of the most difficult challenges of implementing 2D Vis spectroscopy, which is the production of phase stable pulse sequences.

To demonstrate the method, a 128-pixel liquid crystal modulator controlling both phase and amplitude was used to shape a ~50 fs pulse at 800 nm running at a 1-kHz repetition rate. The pulse pair is followed by an ultrashort probe pulse that is spectrally resolved. The delay between the collinear pulses is incremented using phase and amplitude shaping and a 2D Vis spectrum is generated by Fourier transformation, just like 2D IR spectra were generated above. Shown in Fig. 12 are 2D Vis spectra of atomic rubidium vapour. Rb vapor has atomic transitions at 794.76 ($5P_{1/2} \leftarrow 5S_{1/2}$) and 780.03 nm ($5P_{3/2} \leftarrow 5S_{1/2}$) and has been used to test other 2D Vis methodologies since it has very narrow linewidths. The real part of the 2D E spectrum is shown in Fig. 12 and exhibits diagonal peaks and cross peaks as expected. The diagonal peaks appear at $\lambda_{pump} = \lambda_{probe}$ = 780 and 795 nm along with crosspeaks between the two transitions. Shown in Fig. 12b is an expanded plot of the real part for the diagonal peak at $\lambda_{pump} = \lambda_{probe}$ = 780 nm. Well-shaped lineshapes are observed, indicating that the shaper can accurately step the delay time. The linewidths differ along λ_{pump} and λ_{probe}, which is to be expected under our experimental conditions where the linewidth along λ_{probe} is determined by the natural linewidth

convoluted with the spectrometer resolution (~0.65 nm), while the linewidth along λ_{pump} is given by the natural linewidth convoluted by the spectral resolution of the Fourier transform, $1/\tau_{max}$, where τ_{max} is the largest τ and 2 ps here. We also measured the phase stability of the pulse pair generated by the shaper and got $\lambda/67$ over the course of 35 h. This number compares to phase drift of $\lambda/100$ typical of diffractive optics and $\lambda/250$ with HeNe interferometry measurements made over the course of ~5 h.[39,64,65]

In most 2D spectrometers, each of the four pulses traverses an independent delay line whose length must not vary more than a fraction of the wavelength during the experiment. Achieving adequate phase stability with visible laser pulses can be difficult in conventional four wave mixing methods. One approach for stabilizing the pathlengths is to use diffractive optics and phase-compensating mirror arrangements.[39,64] Another is to actively adjust the optical pathlengths using piezocrystals and two sets of HeNe interferometers for feed-back. [65] If the drift is slow enough, then it can be measured and the data corrected.[38] All of these approaches result in high quality multidimensional electronic spectra, on the other hand, it is straightforward to generate phase-locked pulse pairs with a pulse shaper capable of modulating the spectrum of femtosecond pulses, like we have described above. Warren and coworkers collected 2D Vis spectra by using an entirely collinear train of 4 pulses in analogy to the way that 2D NMR spectra are generated using phase cycling.[62] However, the fully collinear geometry necessitates that the signal be measured by some observable other than absorption (*e.g.* fluorescence), since the intense excitation pulses will saturate the detector in a linear absorption arrangement. In contrast, Nelson and coworkers used a two-dimensional pulse shaper to collect 2D Vis spectra in a non-collinear boxcar geometry where all 4 pulses in the pulse train impinge on the sample from different directions.[63] The approach by Nelson and coworkers takes advantage of phase matching that provides background free signal and eliminates the need for phase cycling. However, the two dimensional pulse shaper has very low throughput efficiency owing to the fact that the input laser beam is spatially filtered to obtain the non-collinear geometry and few pixels, which limits the complexity of the shapes that can be generated.

Our method that significantly eases the hurdles associated with collecting 2D Vis spectra. 2D Vis spectra can be measured using commonly available pulse shapers and a partly collinear pump–probe beam geometry. With a pulse shaper and a spectrometer, which many research groups already own, it is a trivial matter to make phase stable pulse trains, thus eliminating difficulties associated with working at short (visible) wavelengths. Furthermore, the beam geometry used in our experiments eliminates the need for complicated phasing procedures. Our method eliminates many of the technical hurdles to implementing 2D Vis spectroscopy, making it possible for many more research groups to exploit this powerful spectroscopy in their research. In fact, it has recently been reported that a Dazzler pulse shaper can be used to collect 2D Vis spectra as well.[53]

Concluding remarks

Femtosecond pulse shaping greatly enhances 2D IR spectroscopy with its ease of use, versatility and speed. Programmable control of pulse shapes makes designing and implementing new pulse sequences just a matter of computer programming. On a daily basis, this method is much easier to maintain than a four-wave mixing setup, since the pulse shaper and the pump/probe geometry requires minimal alignment. In many ways, the ease of alignment and accuracy of the collected data is the greatest attribute of this method. In our experience, much more time can be spent on the application of the technique to scientific questions rather than on technical maintenance of the spectrometer and phasing of the data.

Rapid-scan 2D IR spectroscopy has been made possible by the development of a pulse shaper that operates in the mid-IR. Further advances will be made possible by straightforward improvements in technology. Polarization control has many uses in 2D IR and Vis spectroscopies (see above for a few examples). It is now straightforward to construct polarization pulse shapers in the visible/near-IR,[59,60] and it should be possible to extend these approaches into the mid-IR. Coherent control methodologies can now also be incorporated into multidimensional spectroscopies with simple programming. We showed that mid-IR pulse shaping can be used to selectively enhance vibrational excitation of desired quantum levels, 66 which, if incorporated into a 2D IR pulse sequence, could be used to enhance or eliminate spectral features.67 It should also now be straight-forward to implement 5th and higher-order signals to measure 3D spectra,[68] for example, since addition of laser pulses no longer requires complicated optical alignments but just additional programming. The speed of rapid-scanning 2D IR spectroscopy can be further accelerated with high repetition rate lasers. With current laser technology, it should be straightforward to increase data acquisition by a factor of 30 or more, resulting in higher signal-to-noise spectra and faster kinetics. It is clear that the utility of 2D spectroscopies for studying structures and dynamics will only improve in the coming years.

Biographies

Sang-Hee Shim

Sang-Hee Shim received her bachelor's and master's degree from Seoul National University, Korea. She graduated from the University of Wisconsin-Madison with a PhD degree under the supervision of Martin Zanni. She is currently a Mary Fieser Postdoctoral Fellow at Harvard University.

Martin Zanni

Martin Zanni attended the University of Rochester for his bachelors degrees and the University of California at Berkeley for his PhD. He was a postdoctoral researcher at the University of Pennsylvania with Robin Hochstrasser. He is currently the Meloche-Bascom Associate Professor of Chemistry at the University of Wisconsin-Madison.

Acknowledgments

We thank David Strasfeld for his contributions in developing the mid-IR pulse shaper, Strasfeld and Yun Ling for the 2D IR spectra of hIAPP in section 2 and 6, and Wei Xiong for the polarization scheme in section 7 and the 2D IR spectra in section 5.4. The amyloid sample was provided by Prof. Dan Raleigh at the State University of New York at Stony Brook. Finally, we appreciate Prof. Niels Damrauer and his group at the University of Colorado at Boulders for the collaboration that generated the 2D Vis spectrum in section 8. Various aspects of the research reviewed in this article were funded by the NIH (DK79895), NSF CAREER (CHE-0350518) and the Packard Foundation.

References

1. See articles contained in the Special Issue; Mukamel S, Hochstrasser RM. Chem. Phys 2001;266:135–136.
2. See articles contained in the Special Issue; Hochstrasser RM. Proc. Natl. Acad. Sci. U. S. A 2007;104:14189–14189. [PubMed: 17724335]
3. Cho MH. Chem. Rev 2008;108:1331–1418. [PubMed: 18363410]
4. Barth A, Zscherp C. Q. Rev. Biophys 2002;35:369–430. [PubMed: 12621861]
5. Decatur SM. Acc. Chem. Res 2006;39:169–175. [PubMed: 16548505]
6. Arkin IT. Curr. Opin. Chem. Biol 2006;10:394–401. [PubMed: 16935550]
7. Chung HS, Khalil M, Smith AW, Ganim Z, Tokmakoff A. Proc. Natl. Acad. Sci. U. S. A 2005;102:612–617. [PubMed: 15630083]
8. Kolano C, Helbing J, Kozinski M, Sander W, Hamm P. Nature 2006;444:469–472. [PubMed: 17122853]
9. Mukherjee P, Kass I, Arkin I, Zanni MT. Proc. Natl. Acad. Sci. U. S. A 2006;103:3528–3533. [PubMed: 16505377]
10. Strasfeld DB, Ling YL, Shim S-H, Zanni MT. J. Am. Chem. Soc 2008;130:6698–6699. [PubMed: 18459774]
11. Shim S-H, Strasfeld DB, Fulmer EC, Zanni MT. Opt. Lett 2006;31:838–840. [PubMed: 16544641]
12. Shim S-H, Strasfeld DB, Ling YL, Zanni MT. Proc. Natl. Acad. Sci. U. S. A 2007;104:14197–14202. [PubMed: 17502604]
13. Grumstrup EM, Shim S-H, Montgomery MA, Damrauer NH, Zanni MT. Opt. Express 2007;15:16681–16689. [PubMed: 19550954]
14. Engel GS, Calhoun TR, Read EL, Ahn TK, Mancal T, Cheng YC, Blankenship RE, Fleming GR. Nature 2007;446:782–786. [PubMed: 17429397]
15. Li XQ, Zhang TH, Borca CN, Cundiff ST. Phys. Rev. Lett 2006;96
16. Meyer KA, Besemann DM, Wright JC. Chem. Phys. Lett 2003;381:642–649.
17. Zanni MT, Gnanakaran S, Stenger J, Hochstrasser RM. J. Phys. Chem. B 2001;105:6520–6535.
18. Golonzka O, Khalil M, Demirdoven N, Tokmakoff A. Phys. Rev. Lett 2001;86:2154–2157. [PubMed: 11289878]
19. Hamm P, Lim MH, Hochstrasser RM. J. Phys. Chem. B 1998;102:6123–6138.
20. DeCamp MF, DeFlores L, McCracken JM, Tokmakoff A, Kwac K, Cho M. J. Phys. Chem. B 2005;109:11016–11026. [PubMed: 16852342]
21. Eaves JD, Loparo JJ, Fecko CJ, Roberts ST, Tokmakoff A, Geissler PL. Proc. Natl. Acad. Sci. U. S. A 2005;102:13019–13022. [PubMed: 16135564]
22. Shim S-H, Gupta R, Ling YL, Strasfeld DB, Raleigh DP, Zanni MT. submitted.
23. Kim YS, Liu L, Axelsen PH, Hochstrasser RM. Proc. Natl. Acad. Sci. U. S. A 2008;105:7720–7725. [PubMed: 18499799]
24. Luca S, Yau WM, Leapman R, Tycko R. Biochemistry 2007;46:13505–13522. [PubMed: 17979302]
25. Zhang WM, Chernyak V, Mukamel S. J. Chem. Phys 1999;110:5011–5028.
26. Fulmer EC, Ding F, Mukherjee P, Zanni MT. Phys. Rev. Lett 2005;94:067402. [PubMed: 15783774]
27. Fulmer EC, Mukherjee P, Krummel AT, Zanni MT. J. Chem. Phys 2004;120:8067–8078. [PubMed: 15267726]
28. Khalil M, Demirdoven N, Tokmakoff A. Phys. Rev. Lett 2003;90:047401. [PubMed: 12570457]
29. Asbury JB, Steinel T, Fayer MD. J. Lumin 2004;107:271–286.
30. Cervetto V, Helbing J, Bredenbeck J, Hamm P. J. Chem. Phys 2004;121:5935–5942. [PubMed: 15367022]
31. Mukamel, S. Principles of Nonlinear Spectroscopy. New York: Oxford University Press; 1995.
32. Hamm, P.; Hochstrasser, RM. Ultrafast Infrared and Raman Spectroscopy. Fayer, MD., editor. New York: Marcel Dekker Inc.; 2001. p. 273-347.
33. Likforman JP, Joffre M, ThierryMieg V. Opt. Lett 1997;22:1104–1106. [PubMed: 18185765]

34. Woutersen S, Hamm P. J. Phys.: Condens. Matter 2002;14:R1035–R1062.
35. Asplund MC, Zanni MT, Hochstrasser RM. Proc. Natl. Acad. Sci. U. S. A 2000;97:8219–8224. [PubMed: 10890905]
36. While slower, the technique may have higher sensitivity when the data is colleted in the time domain because there is no signal loss from the spectrometer grating, although this assertion has not been explored quantitatively.
37. Volkov V, Schanz R, Hamm P. Opt. Lett 2005;30:2010–2012. [PubMed: 16092249]
38. Ding F, Mukherjee P, Zanni M. Opt. Lett 2006;31:2918–2920. [PubMed: 16969422]
39. Brixner T, Mancal T, Stiopkin IV, Fleming GR. J. Chem. Phys 2004;121:4221–4236. [PubMed: 15332970]
40. Cowan ML, Ogilvie JP, Miller RJD. Chem. Phys. Lett 2004;386:184–189.
41. Shim S-H, Strasfeld DB, Zanni MT. Opt. Express 2006;14:13120–13130. [PubMed: 19532209]
42. Hillegas CW, Tull JX, Goswami D, Strickland D, Warren WS. Opt. Lett 1994;19:737–739. [PubMed: 19844429]
43. Weiner AM. Rev. Sci. Instrum 2000;71:1929–1960.
44. Hernandez, G. Fabry-Perot Interferometers. New York: Cambridge University Press; 1986.
45. Witte T, Yeston JS, Motzkus M, Heilweil EJ, Kompa K-L. Chem. Phys. Lett 2004;392:156–161.
46. Ernst, RR.; Bodenhausen, G.; Wokaun, A. Principles of Nuclear Magnetic Resonance in One and Two Dimensions. Oxford: Oxford University Press; 1987.
47. Albrecht AW, Hybl JD, Faeder SMG, Jonas DM. J. Chem. Phys 1999;111:10934–10956.
48. Marshall, AG.; Verdun, FR. Fourier Transforms in NMR, Optical, and Mass Spectroscopy: A User's Handbook. New York: Elsevier Science Publishers; 1990.
49. Jaikaran E, Higham CE, Serpell LC, Zurdo J, Gross M, Clark A, Fraser PE. J. Mol. Biol 2001;308:515–525. [PubMed: 11327784]
50. Ge NH, Zanni MT, Hochstrasser RM. J. Phys. Chem. A 2002;106:962–972.
51. Cheng YC, Fleming GR. J. Phys. Chem. A 2008;112:4254–4260. [PubMed: 18376878]
52. de Boeij WP, Pshenichnikov MS, Wiersma DA. Chem. Phys 1998;233:287–309.
53. Myers J, Lewis KLM, Tekavec PF, Ogilvie JP. Opt. Express 2008;16:17420–17428. [PubMed: 18958024]
54. Nee MJ, McCanne R, Kubarych KJ, Joffre M. Opt. Lett 2007;32:713–715. [PubMed: 17308611]
55. Jayasinghe SA, Langen R. Biochemistry 2005;44:12113–12119. [PubMed: 16142909]
56. Knight JD, Hebda JA, Miranker AD. Biochemistry 2006;45:9496–9508. [PubMed: 16878984]
57. Zanni MT, Ge NH, Kim YS, Hochstrasser RM. Proc. Natl. Acad. Sci. U. S. A 2001;98:11265–11270. [PubMed: 11562493]
58. Xiong W, Zanni MT. Opt. Lett 2008;33:1371–1373. [PubMed: 18552963]
59. Brixner T, Gerber G. Opt. Lett 2001;26:557–559. [PubMed: 18040384]
60. Polachek L, Oron D, Silberberg Y. Opt. Lett 2006;31:631–633. [PubMed: 16570421]
61. DeCamp ME, Tokmakoff A. Opt. Lett 2005;30:1818–1820. [PubMed: 16092356]
62. Tian PF, Keusters D, Suzaki Y, Warren WS. Science 2003;300:1553–1555. [PubMed: 12791987]
63. Vaughan JC, Hornung T, Stone KW, Nelson KA. J. Phys. Chem. A 2007;111:4873–4883. [PubMed: 17552490]
64. Goodno GD, Dadusc G, Miller RJD. J. Opt. Soc. Am. B 1998;15:1791–1794.
65. Zhang TH, Borca CN, Li XQ, Cundiff ST. Opt. Express 2005;13:7432–7441. [PubMed: 19498768]
66. Strasfeld DB, Shim S-H, Zanni MT. Phys. Rev. Lett 2007;99
67. Abramavicius D, Mukamel S. J. Chem. Phys 2004;120:8373–8378. [PubMed: 15267760]
68. Ding F, Zanni MT. Chem. Phys 2007;341:95–105.

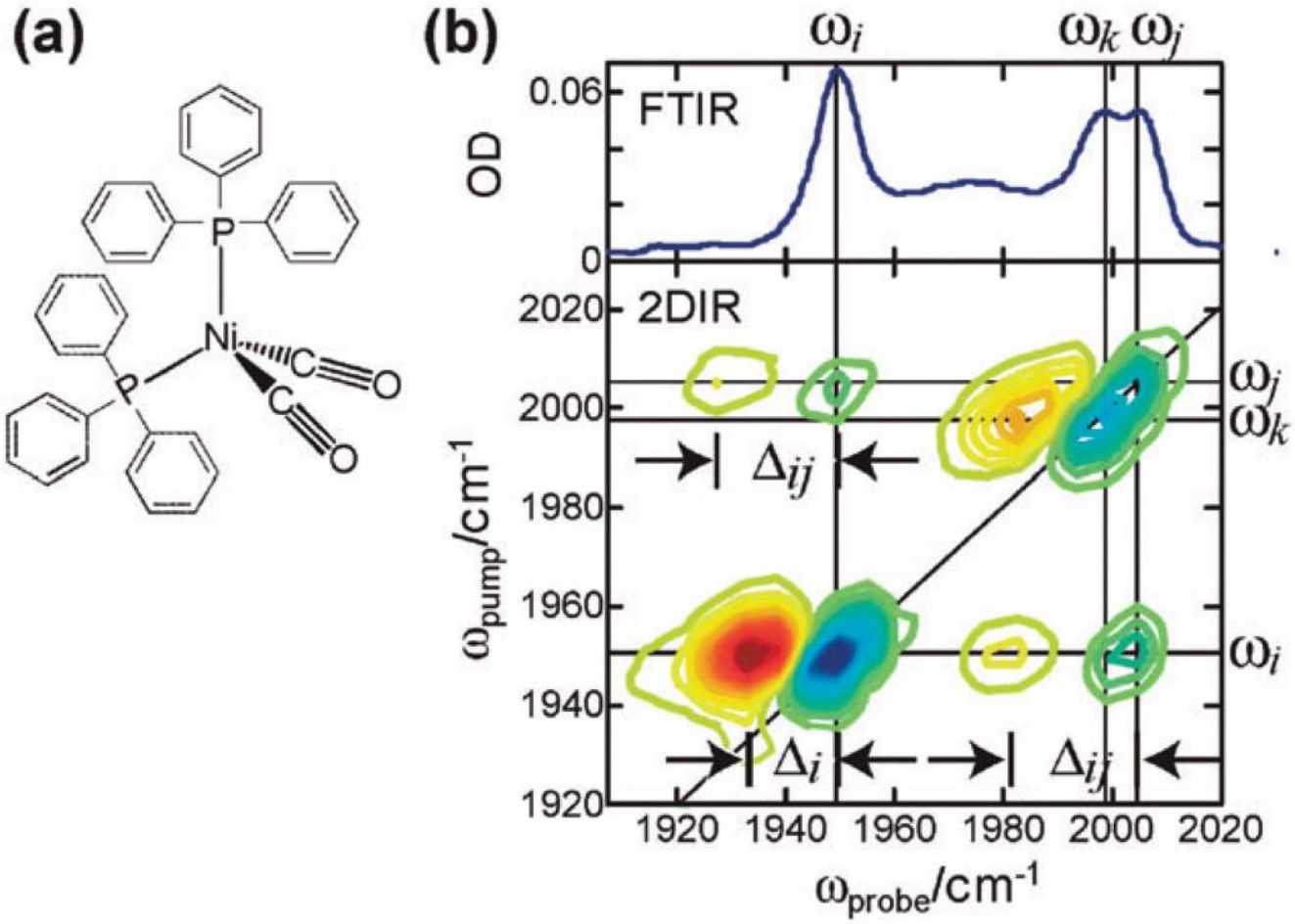

Fig. 1.

2D IR spectrum of a coupled system (a) Structure of $Ni_2(PPh_3)_2(CO)_2$. (b) 1D and 2D IR spectra of $Ni_2(PPh_3)_2(CO)_2$ in THF–hexane (1 : 3) with two coupled vibrational modes at ω_i and ω_j and an uncoupled molds at ω_k. Anharmonicities are shown for the diagonal doublet at ω_i (Δ_i) and the off-diagonal doublet between ω_i and ω_j (Δ_{ij}). Vertical and horizontal lines highlights the fundamental frequencies of ω_i, ω_j and ω_k, and a diagonal line is drawn though the fundamental frequencies. Negative peaks are shown in blue and positive peaks in red.

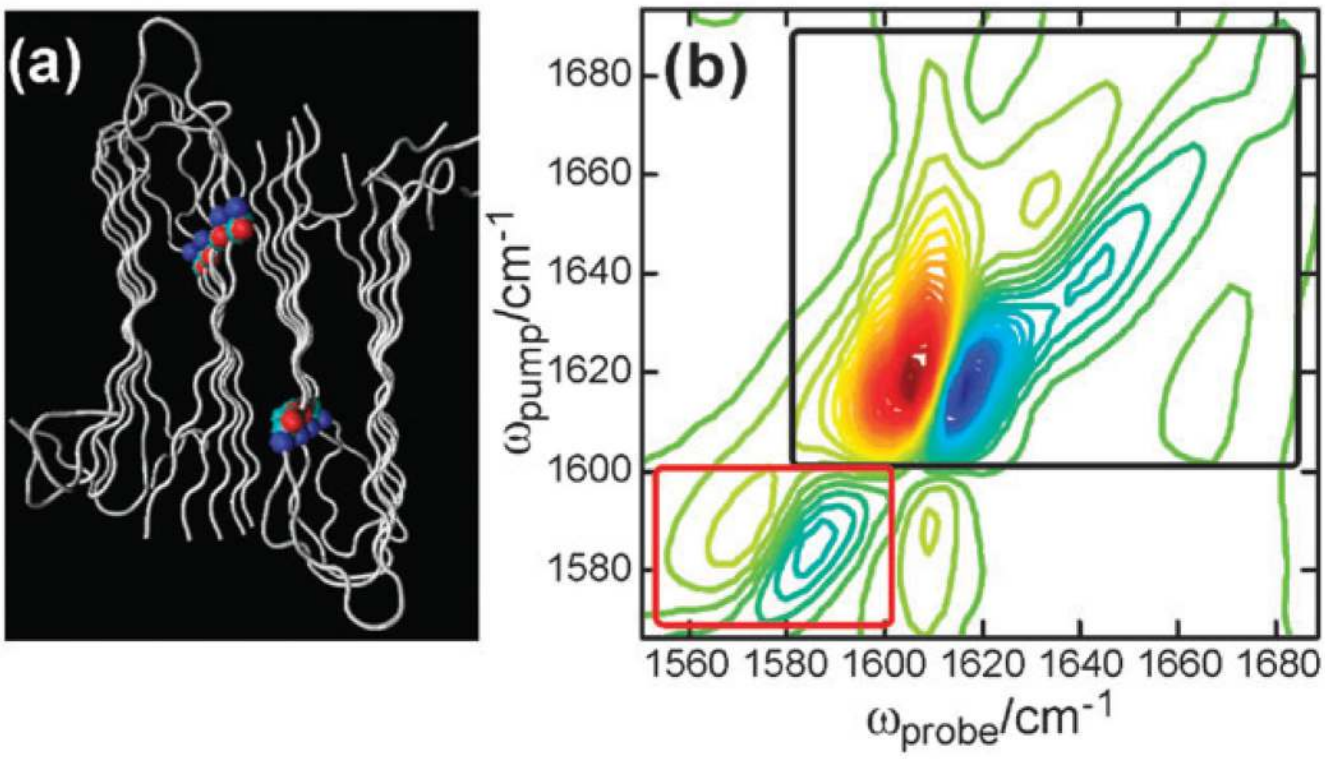

Fig. 2.

2D IR spectrum of the amyloid fibrils from hIAPP peptides isotope-labeled at Leu27. (a) Proposed structure of a hIAPP fibril containing five stacks of two hairpins at each layer. The backbone atoms of Leu27 are coloured in cyan for carbon, red for oxygen, and blue for nitrogen. (b) 2D IR spectrum of the fibrils from the labelled peptides. The doublet at ω_{probe} = 1550–1600 cm^{-1} from the $^{13}C^{18}O$ label (red box) is spectrally separated from the remainder of the peptide backbones in $^{12}C^{16}O$ (black box) and reflects the environment of the single residue.

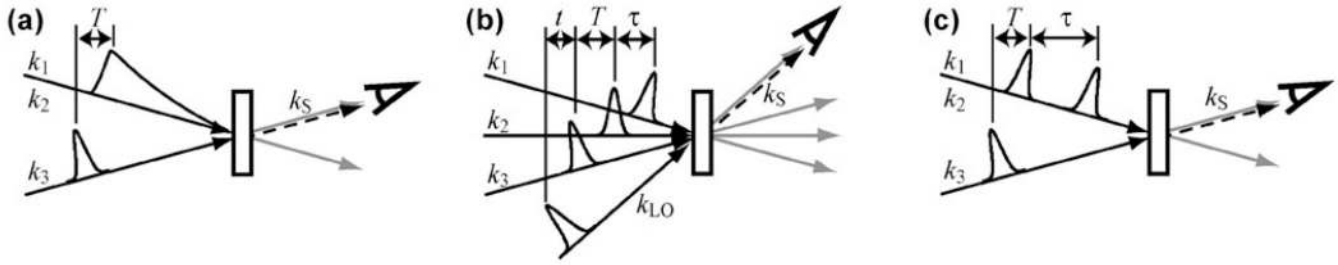

Fig. 3.
Schematic layouts of 2D IR experiments: (a) hole-burning method; (b) pulsed four-wave mixing method; and (b) partly collinear method using a pulse shaper.

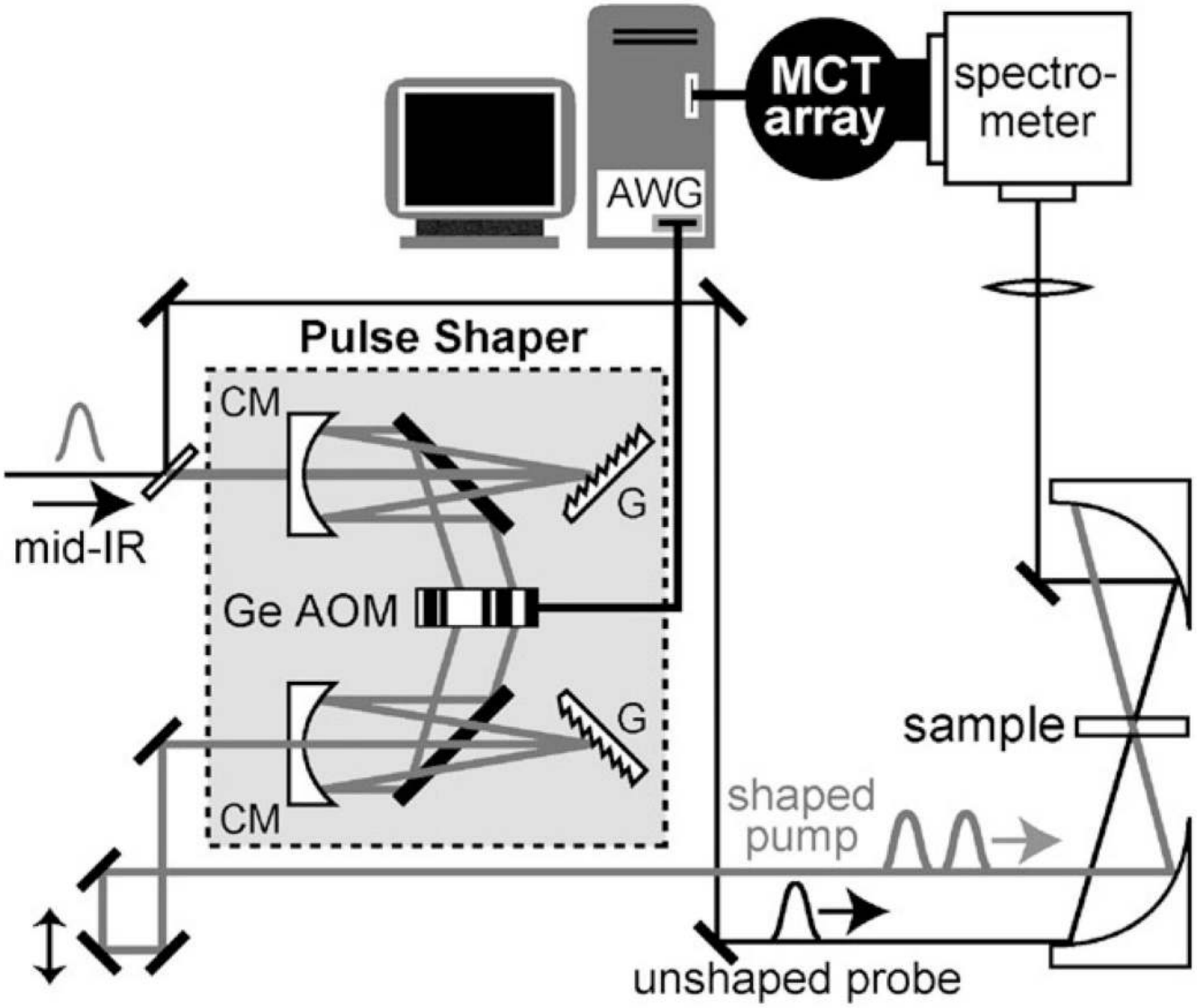

Fig. 4.

The experimental setup of the automated 2D IR includes a mid-IR pulse shaper (gray area enclosed with a dashed line) and a pump–probe spectrometer. The pulse shaper consists of two gratings (G) and cylindrical mirrors (CM) in a 4-*f* geometry as well as a germanium acousto-optic modulator (Ge AOM) controlled by an arbitrary waveform generator (AWG) equipped on a computer. The shaped beam serves as a pump beam (thick gray line) and a small portion of the unshaped beam is used as a probe beam (solid black line). The probe spectrum is measured with a mercury cadmium telluride (MCT) array detector equipped to a spectrometer.

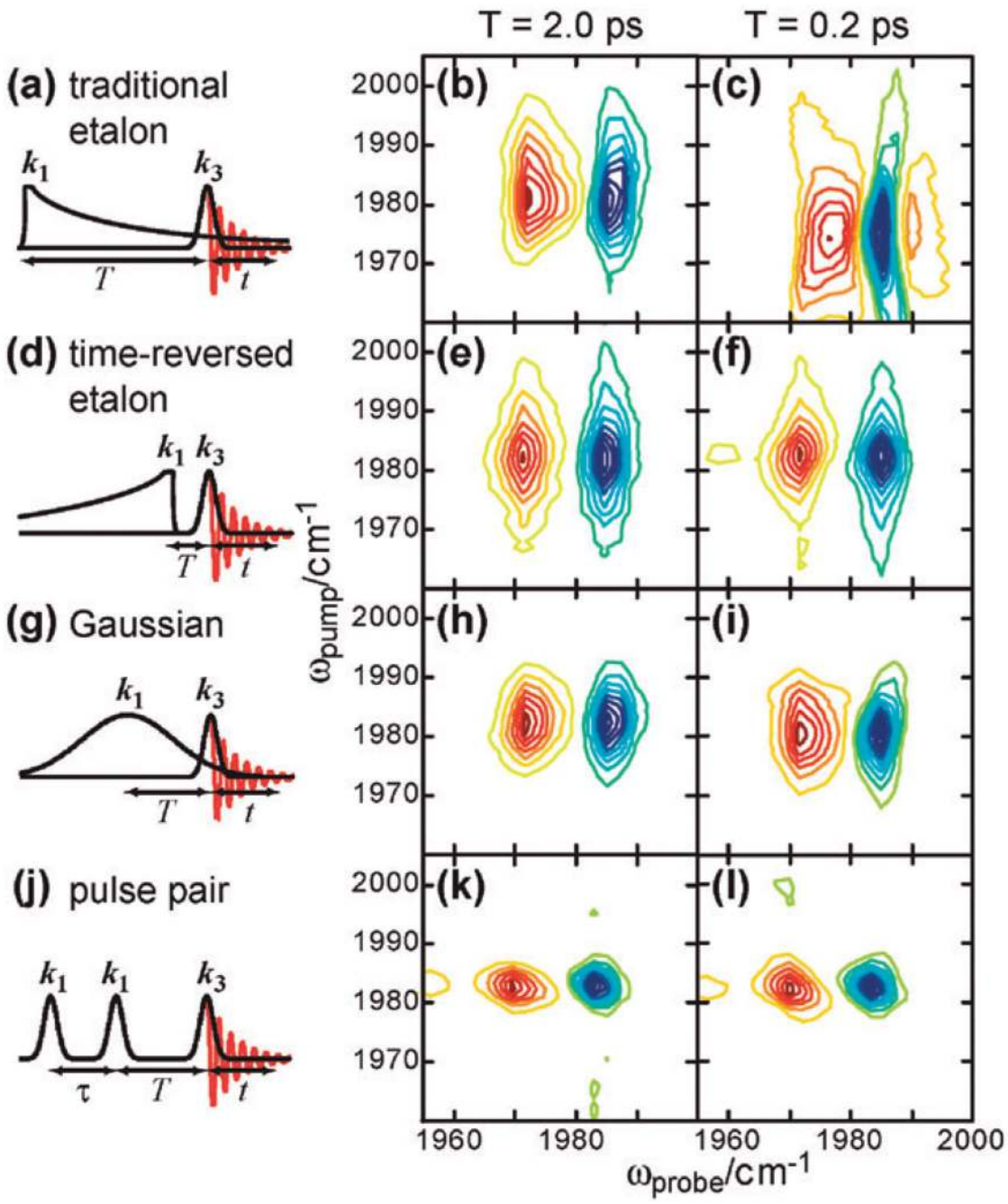

Fig. 5.

Various pulse shapes to collect 2D IR spectra. Pulse sequences in time domain: (a) a traditional etalon; (d) time-reversed etalon; (g) a Gaussian; (j) a pulse pair. 2D IR spectra of $W(CO)_6$ in hexane at $T = 2.0$ and 0.2 ps using the pulse shapes: (b–c) traditional etalon; (e–f) time-reversed etalon; (h–i) Gaussian; (k–l) a pulse pair. Each row shows spectra taken from the same pump shape, while each column aligns spectra with the same T.

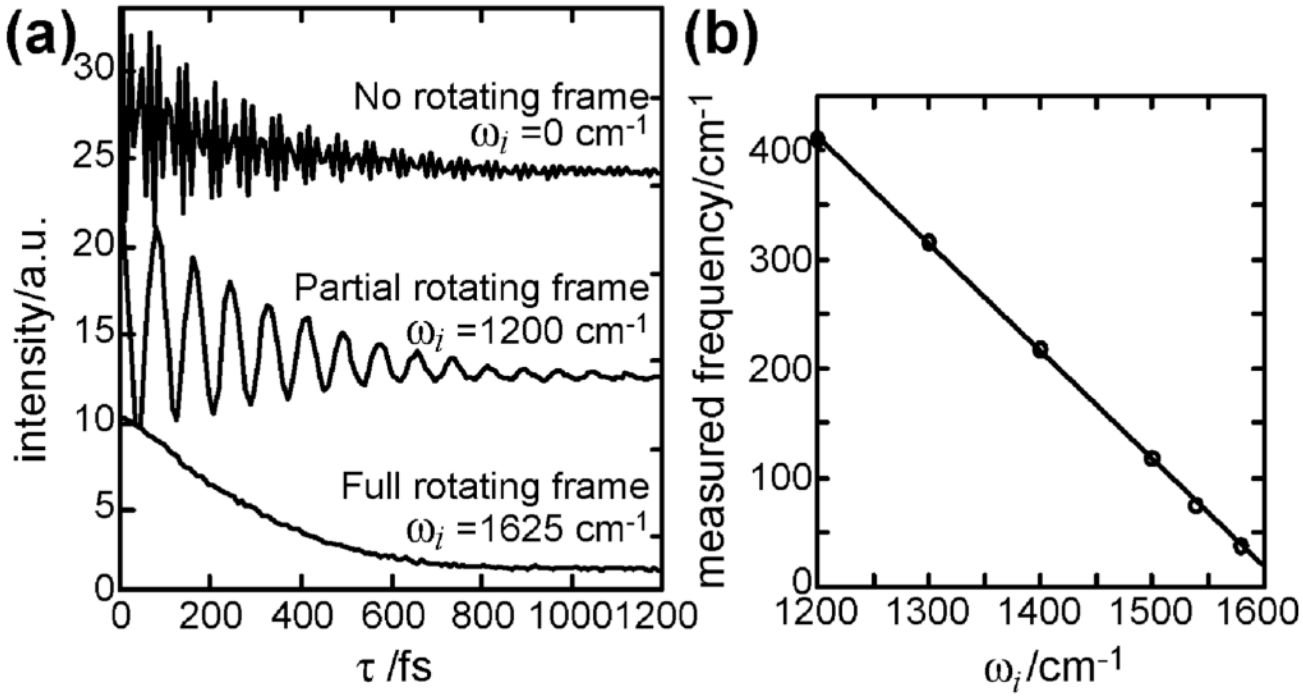

Fig. 6.

The rotating frame demonstrated with the amide I mode of *N*-acetylamide (NMA) by incrementing the relative phase, $\Delta \phi_{12}$, in proportion to τ. (a) Time scans at ω_{probe} = 1625 cm^{-1} by using ω_i = 0, 1200 and 1625 cm^{-1} for no, partial and full rotating frame, respectively. (b) The measured frequency after Fourier-transforming the time scans similar to the ones in Fig. 6a plotted with various ω_is used for partial rotating frames.

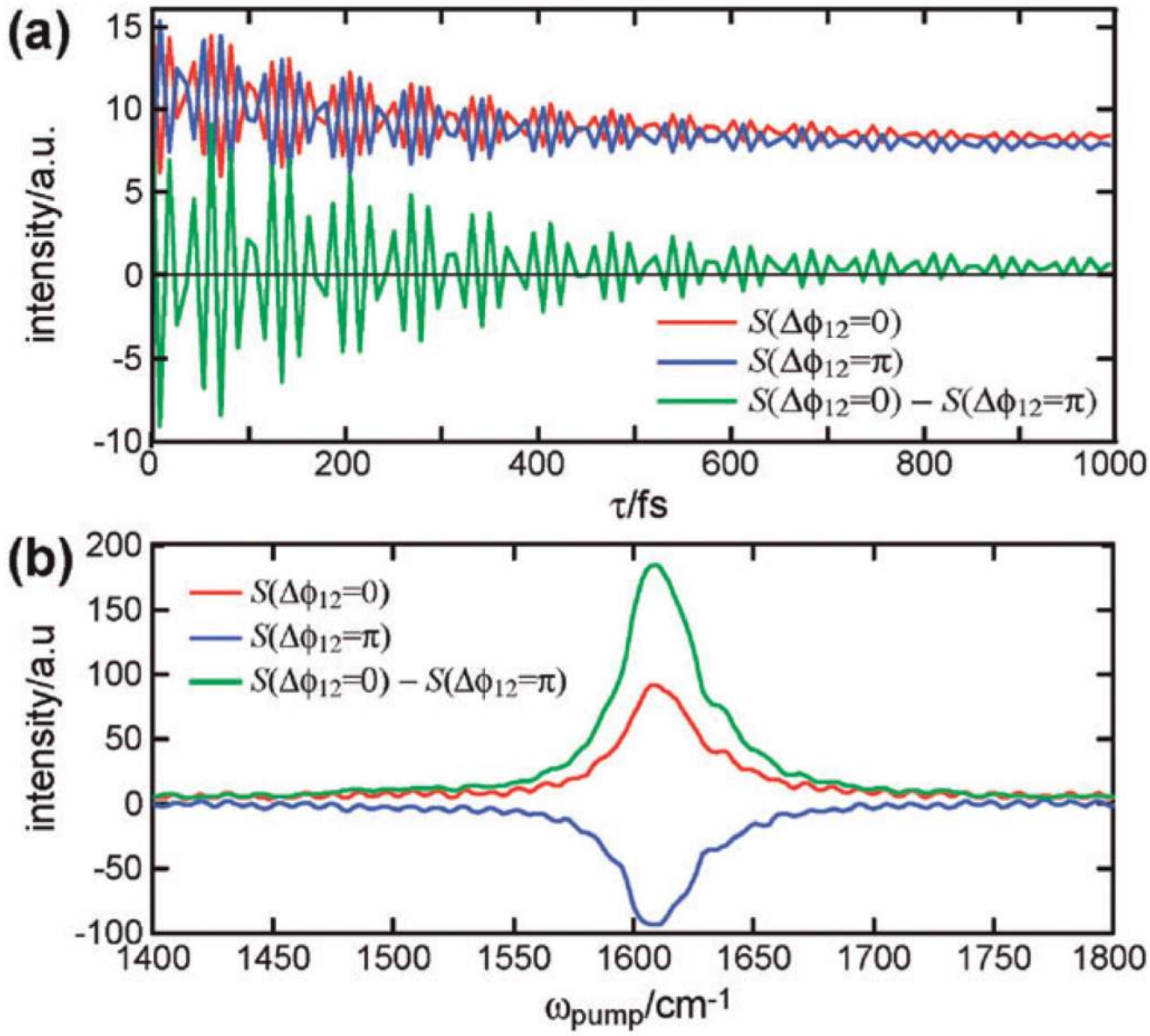

Fig. 7.

Removing backgrounds from transient absorption using a phase cycling scheme for the amide I mode of NMA in D_2O. (a) Time scans at $\omega_{probe} = 1625\ cm^{-1}$ when $\Delta\phi = 0$ (red) and $\Delta\phi = \pi$ (blue), which are 180° out-of-phase, and the subtracted product of the two scans (green). (b) Fourier transforms of the time scans in (a). These are equivalent to the slices along ω_{pump} of 2D IR spectra.

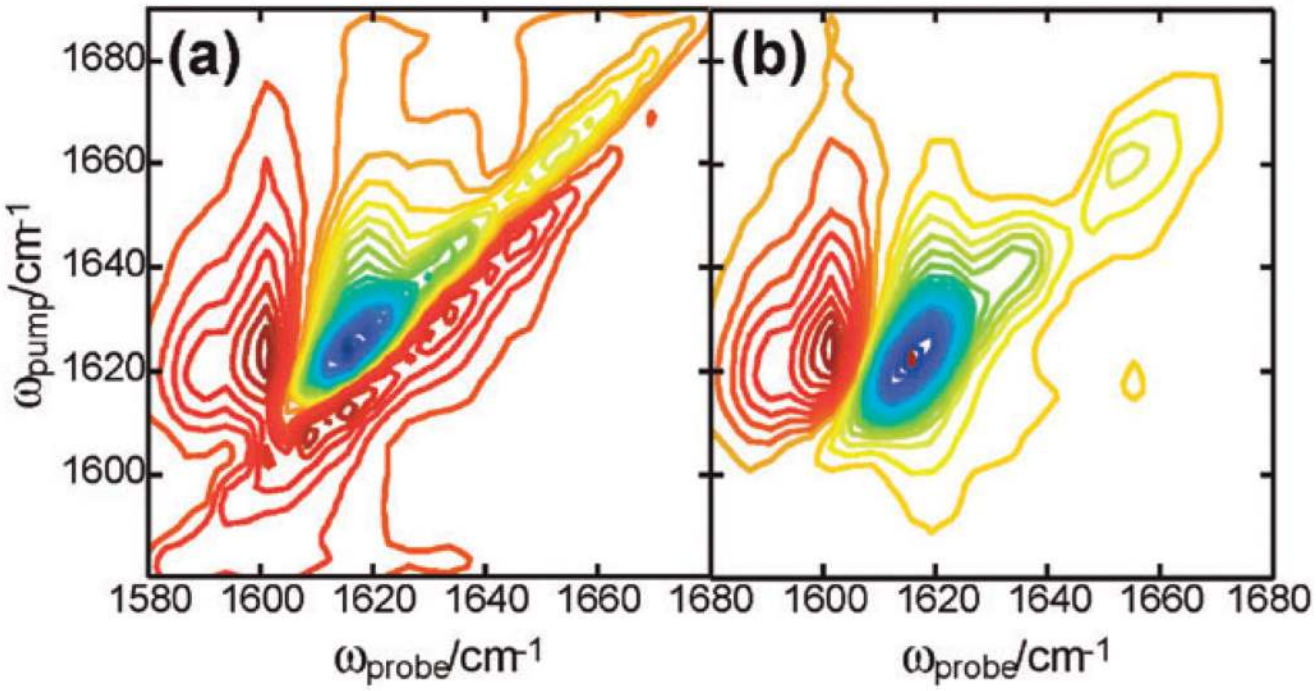

Fig. 8.

Removing scatter by incrementing the absolute phase of the pump pulses. 2D IR spectra of hIAPP fiber in D_2O were collected with (a) no phase increments and (b) $\omega_i = 1800\ cm^{-1}$. The scatter which appears along the diagonal in (a) is now absent in (b).

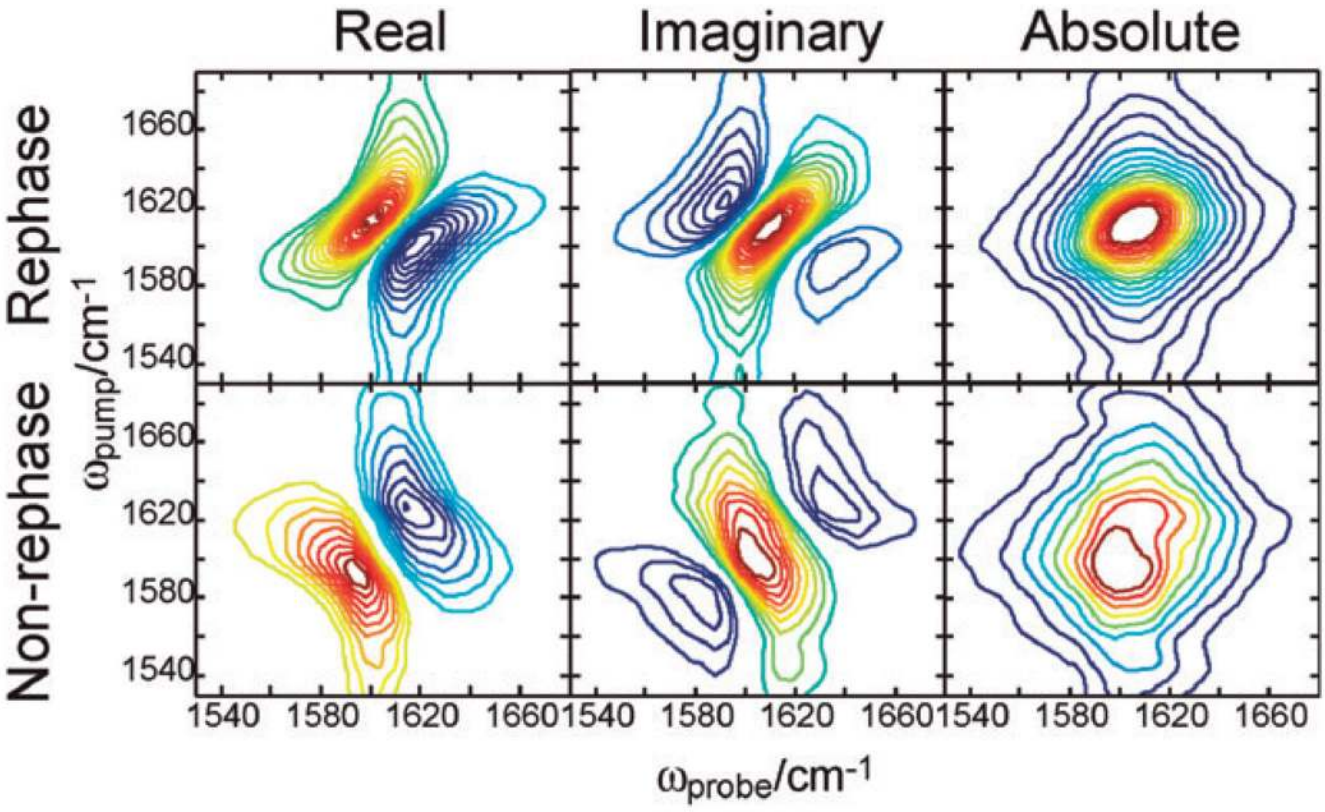

Fig. 9.

Extracting the rephasing and non-rephasing 2D IR spectra for amide I mode of NMA in D_2O by cycling the relative phase of the pump pulses. The columns contain real, imaginary and absolute value spectra as indicated. The top row shows components of the rephasing signal. The bottom row displays the non-rephasing spectra.

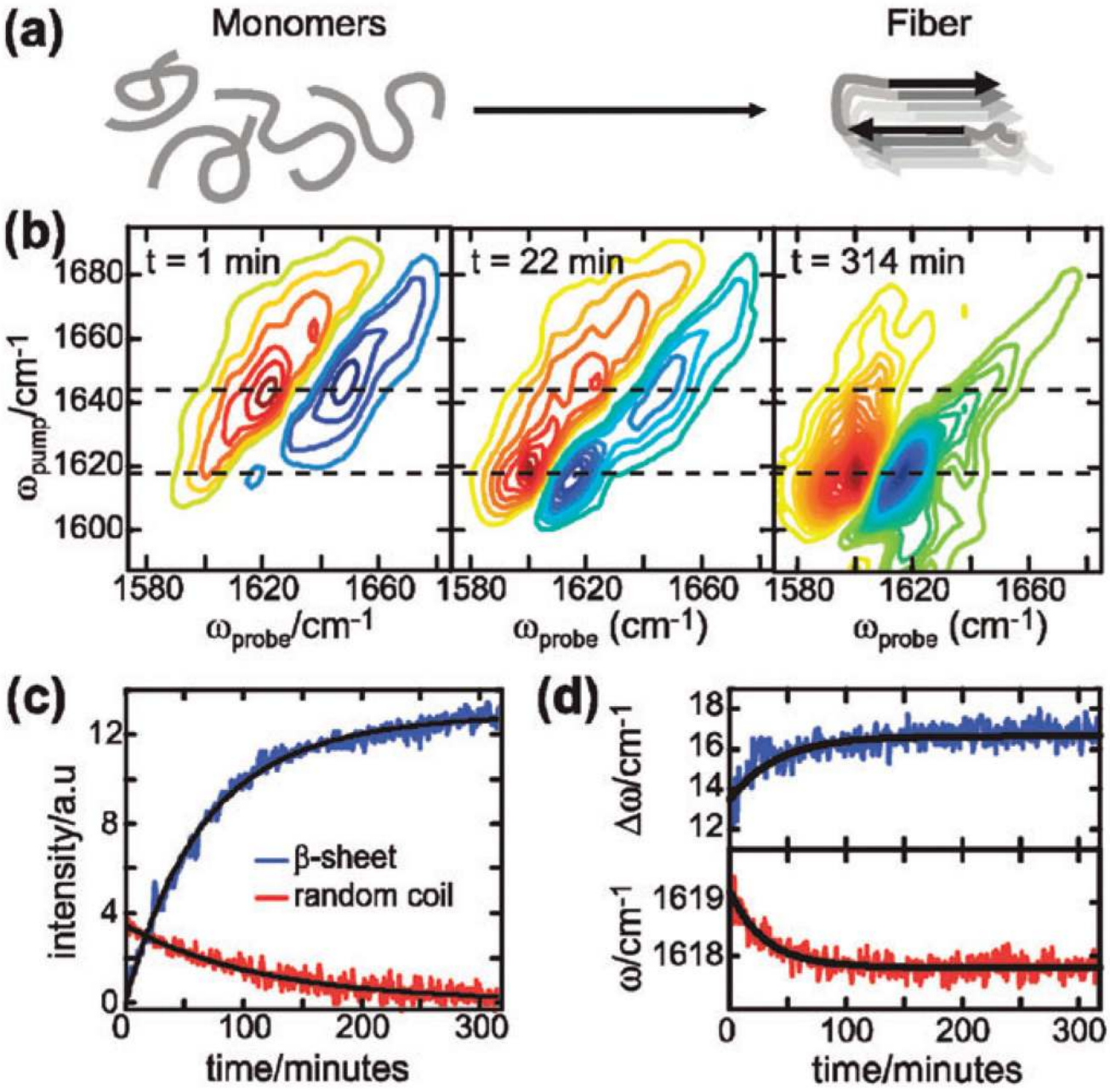

Fig. 10.

On-the-fly 2D IR experiments tracking hIAPP amyloid formation. (a) A schematic of amyloid formation from random coil to fibril rich in β-sheet. (b) Three representative 2D IR spectra at folding times *t*= 1, 22, and 314 min over the course of the aggregation process. (c) Kinetics curves of the β-sheet and the random coil. (d) Changes in the lineshape (Δω) and the frequency (ω) of the beta-sheet feature at 1618 cm^{-1}.

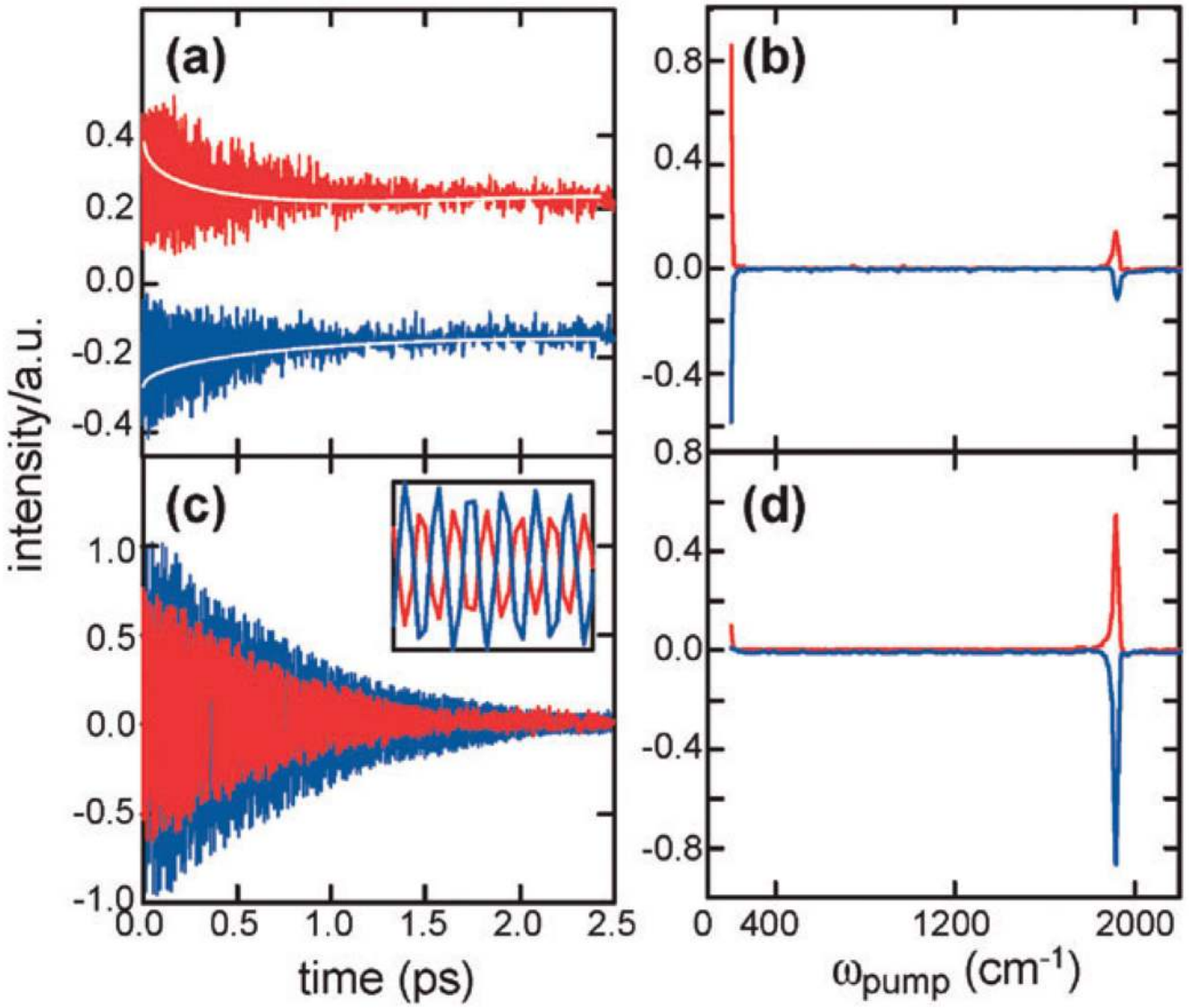

Fig. 11.

Creating background-free and intensified signal by controlling polarizations of the four pulses used for collecting 2D IR spectra. Time and frequency domain data were collected for the antisymmetric stretch of acetic acid in chloroform measured with polarization combinations of (a–b) *XXYY* and (c–d) *XYXY*: (a and c) are the time-domain data at ω_{probe} = 1703 (blue) and 1716 (red) cm^{-1}; (b and d) are the corresponding frequency-domain data.

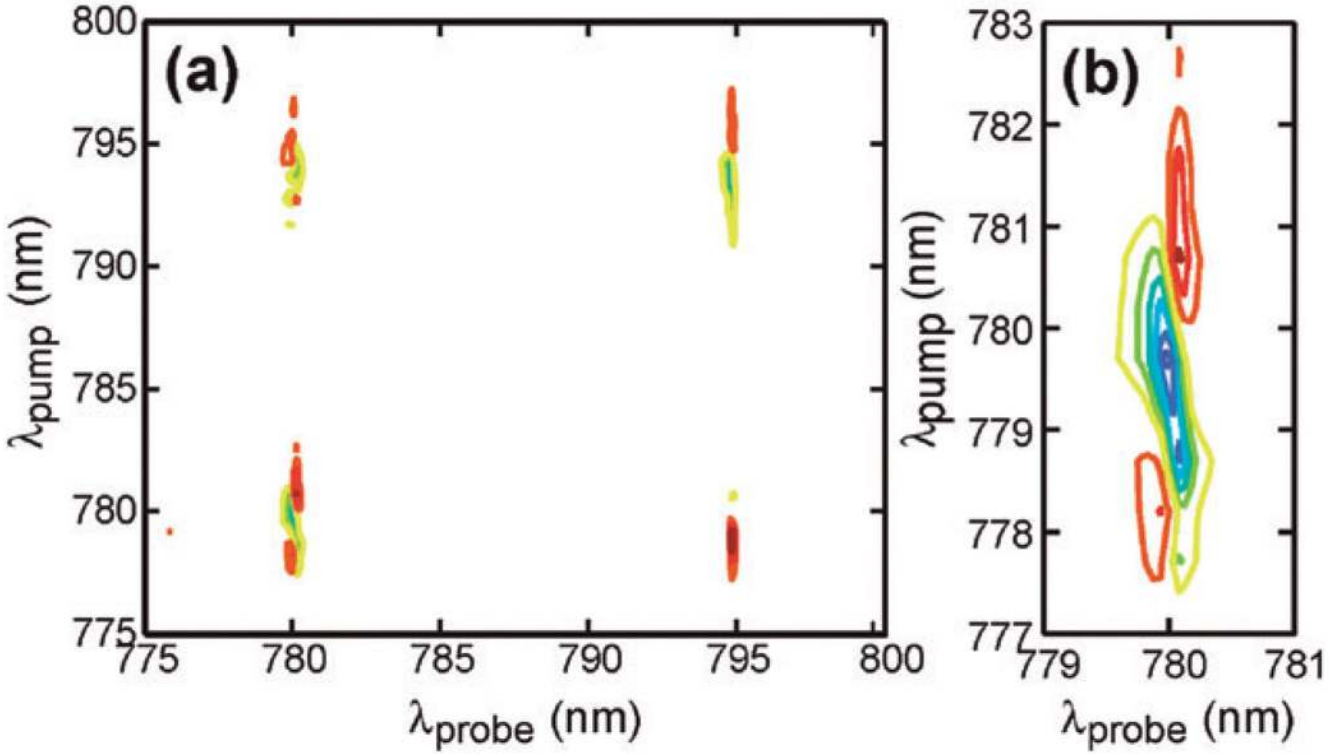

Fig. 12.

2D Vis spectra of atomic Ru vapour collected by a partly collinear setup combined with a standard liquid crystal modulator: (a) real part over $\lambda_{pump} = \lambda_{probe} = 775\sim800$ nm; (b) expanded plots of real part for the diagonal peaks at $\lambda_{pump} = \lambda_{probe} = 780$ nm.